Article

Cell Stem Cell

GPD1 Specifically Marks Dormant Glioma Stem Cells with a Distinct Metabolic Profile

Graphical Abstract

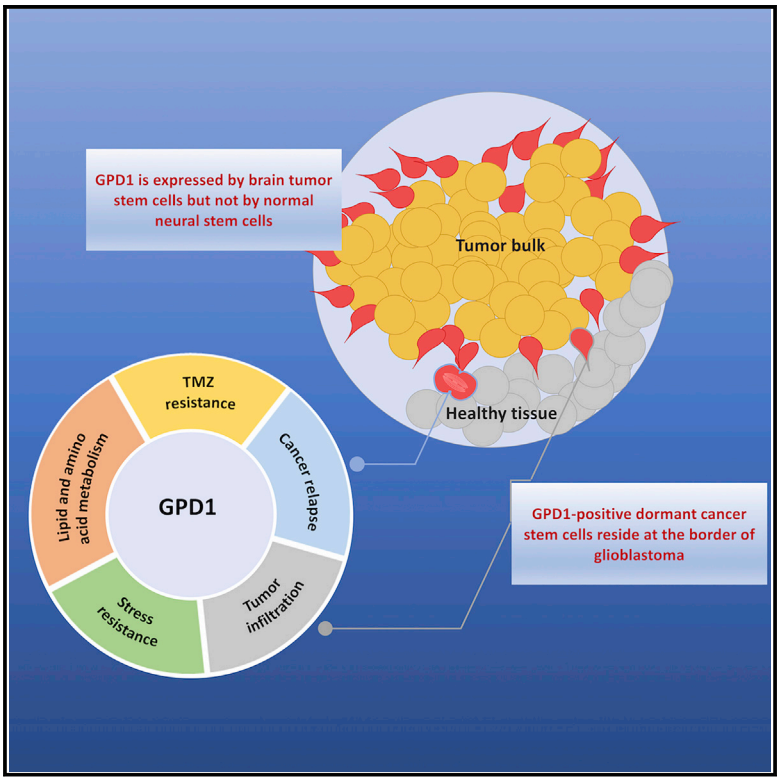

Authors

Patricia Rusu, Chunxuan Shao, Anna Neuerburg, ..., Christel Herold-Mende, Bernhard Radlwimmer, Hai-Kun Liu

Correspondence

l.haikun@dkfz.de

In Brief

Identifying markers specifically expressed by brain tumor stem cells (BTSCs) may enable specific therapies that spare their normal tissue-resident counterparts. Rusu et al. identify GPD1 as a specific marker for dormant and chemoresistant BTSCs and show that targeting GPD1 disrupts BTSC maintenance and extends survival.

Highlights

- GPD1 is expressed in brain tumor stem cells (BTSCs) but not normal neural stem cells
- GPD1^{+} BTSCs are dormant but induced to divide by chemotherapy
- GPD1 inhibition blocks BTSC maintenance and prolongs survival
- GPD1 regulates essential metabolic and molecular programs in glioblastoma

Rusu et al., 2019, Cell Stem Cell *25*, 241–257
August 1, 2019
https://doi.org/10.1016/j.stem.2019.06.004

CellPress

Cell Stem Cell
Article

GPD1 Specifically Marks Dormant Glioma Stem Cells with a Distinct Metabolic Profile

Patricia Rusu,[1,10] Chunxuan Shao,[1] Anna Neuerburg,[1] Azer Aylin Acikgöz,[1] Yonghe Wu,[2] Peng Zou,[1] Prasad Phapale,[3] Tchirupura S. Shankar,[1] Kristina Döring,[4] Steffen Dettling,[5] Huiqin Körkel-Qu,[1] Gözde Bekki,[1] Barbara Costa,[6] Te Guo,[6] Olga Friesen,[1] Magdalena Schlotter,[2] Mathias Heikenwalder,[7] Darjus F. Tschaharganeh,[8,9] Bernd Bukau,[4] Günter Kramer,[4] Peter Angel,[6] Christel Herold-Mende,[5] Bernhard Radlwimmer,[2] and Hai-Kun Liu[1,11,*]

[1]Division of Molecular Neurogenetics, German Cancer Research Center (DKFZ), DKFZ-ZMBH Alliance, Im Neuenheimer Feld 280, Heidelberg 69120, Germany

[2]Division of Molecular Genetics, German Cancer Research Center (DKFZ), Im Neuenheimer Feld 280, Center for Personalized Oncology, DKFZ-HIPO, German Cancer Research Center (DKFZ), Im Neuenheimer Feld 280, 69120 Heidelberg, Germany

[3]Metabolomics Core Facility, European Molecular Biology Laboratory, Heidelberg 69117, Germany

[4]Center for Molecular Biology of Heidelberg University (ZMBH), DKFZ-ZMBH Alliance, Im Neuenheimer Feld 282, Heidelberg 69120, Germany

[5]Division of Neurosurgical Research, Department of Neurosurgery, University of Heidelberg, Im Neuenheimer Feld 400, Heidelberg 69120, Germany

[6]Division of Signal Transduction and Growth Control, German Cancer Research Center (DKFZ), DKFZ-ZMBH Alliance, Im Neuenheimer Feld 280, Heidelberg 69120, Germany

[7]Division of Chronic Inflammation and Cancer, German Cancer Research Center (DKFZ), Im Neuenheimer Feld 242, 69120 Heidelberg, Germany

[8]Helmholtz-University Group 'Cell Plasticity and Epigenetic Remodeling', German Cancer Research Center (DKFZ), Im Neuenheimer Feld 280, Heidelberg 69120, Germany

[9]Institute of Pathology, University Hospital, Heidelberg, Im Neuenheimer Feld 224, Heidelberg 69120, Germany

[10]Present address: Department of Biochemistry and Molecular Biology, Division of Nutrient Metabolism and Signaling, Monash University, 23 Innovation Walk, Clayton, VIC 3800, Australia

[11]Lead Contact

*Correspondence: l.haikun@dkfz.de

https://doi.org/10.1016/j.stem.2019.06.004

SUMMARY

Brain tumor stem cells (BTSCs) are a chemoresistant population that can drive tumor growth and relapse, but the lack of BTSC-specific markers prevents selective targeting that spares resident stem cells. Through a ribosome-profiling analysis of mouse neural stem cells (NSCs) and BTSCs, we find glycerol-3-phosphate dehydrogenase 1 (GPD1) expression specifically in BTSCs and not in NSCs. GPD1 expression is present in the dormant BTSC population, which is enriched at tumor borders and drives tumor relapse after chemotherapy. GPD1 inhibition prolongs survival in mouse models of glioblastoma in part through altering cellular metabolism and protein translation, compromising BTSC maintenance. Metabolomic and lipidomic analyses confirm that GPD1$^+$ BTSCs have a profile distinct from that of NSCs, which is dependent on GPD1 expression. Similar GPD1 expression patterns and prognostic associations are observed in human gliomas. This study provides an attractive therapeutic target for treating brain tumors and new insights into mechanisms regulating BTSC dormancy.

INTRODUCTION

The discovery of cancer stem cells (CSCs) and the formulation of the CSC hypothesis suggest the existence of a cellular hierarchy in malignant tissues (Clarke et al., 2006; Kreso and Dick, 2014; Lapidot et al., 1994; Magee et al., 2012; Reya et al., 2001). This hypothesis also implies that targeting CSCs is the prerequisite to control tumor progression as the CSCs serve as the root for tumorigenesis and relapse. One difficulty of targeting CSCs is that these cells hijack self-renewal pathways, which are required for the maintenance of normal stem cells (Clevers, 2011; Vescovi et al., 2006). Thus, the identification of essential CSC-specific regulators will improve our understanding of the regulation of cancer stemness and provide insights into novel therapy designs against CSCs.

Glioblastoma (GBM) remains to be one of the most lethal solid tumors (Stupp et al., 2017; Wen and Kesari, 2008). Currently, there is no effective targeted therapy for glioblastoma patients. While the chemotherapeutic temozolomide (TMZ) reduces tumor size by targeting fast dividing tumor cells, so-called brain tumor stem cells (BTSCs) are quiescent, slow dividing, resistant to TMZ and irradiation treatment, and get activated during tumor relapse (Bao et al., 2006; Chen et al., 2012; Zhu et al., 2014). Cell ablation or inhibition of self-renewal pathways resulted in a prolonged survival in tumor-bearing mice suggesting that BTSCs are suitable targets in glioblastoma (Chen et al., 2012; Zhu et al., 2014). Many markers have been proposed for BTSCs, e.g., CD133 (Singh et al., 2003, 2004), Tlx/Nr2e1(Zhu et al., 2014), SOX2 (Hemmati et al., 2003), OLIG2 (Ligon et al., 2007), and NESTIN (Tunici et al., 2004). However, these markers are also expressed in NSCs. Here, we performed RNA sequencing and ribosome profiling to compare molecular differences between mouse BTSCs and mouse neural stem cells (NSCs) isolated from

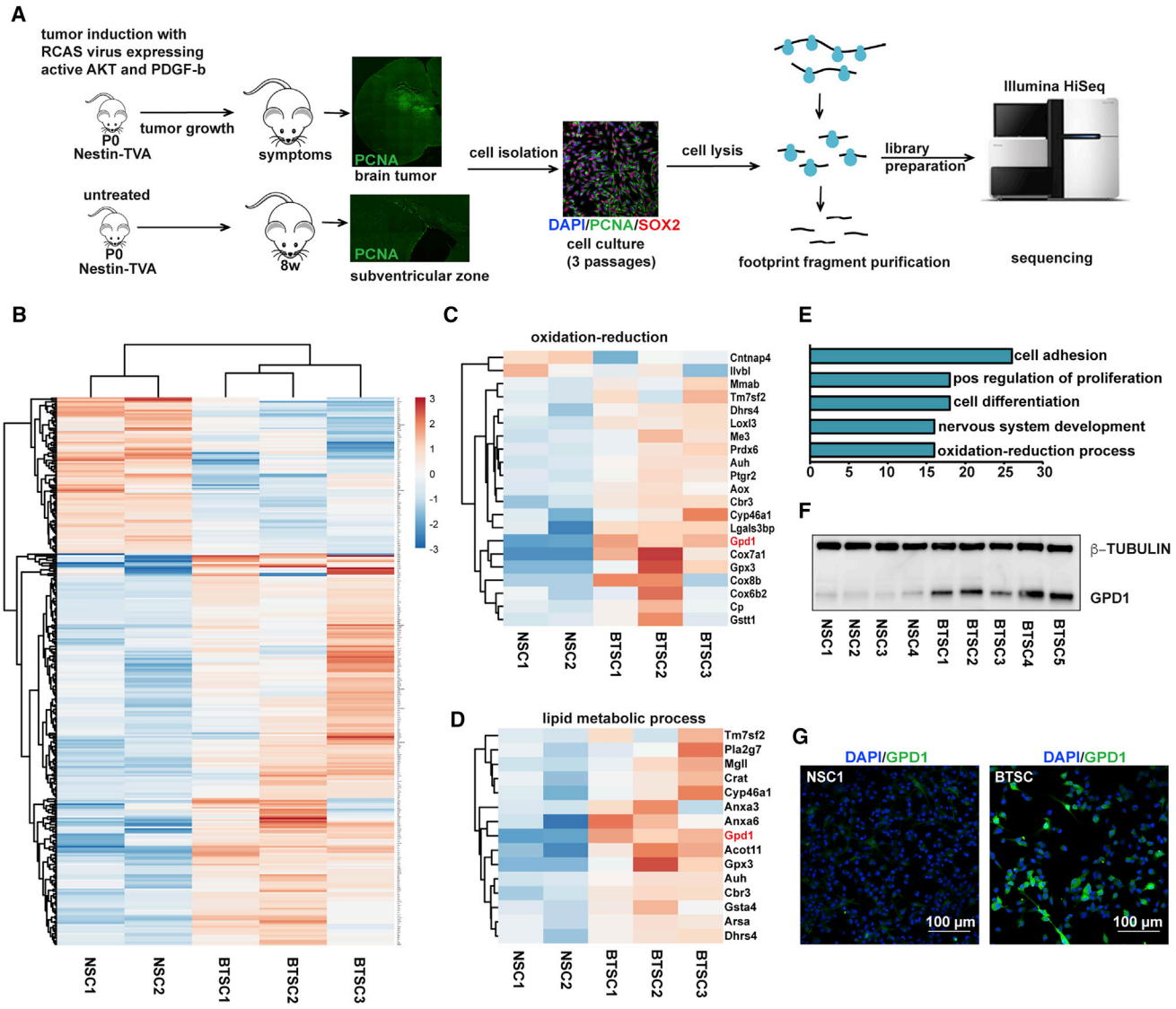

Figure 1. Ribosome Profiling Analysis of BTSCs and NSCs

(A) Experimental design: after induction of brain tumors in Ntv-a mice, BTSCs and NSCs were freshly isolated from mice and kept in culture for expansion. The ribosome footprints were purified and sent for sequencing.

(B) Hierarchical clustering of the ribosome profiling results demonstrates molecular differences between NSCs and BTSCs (log2 fold changes, median centered).

(C) Genes involved in oxidation-reduction are upregulated in BTSCs

(D) Genes involved in lipid metabolism are upregulated in BTSCs; note that GPD1 is upregulated in BTSCs (red).

(E) GO analysis identifies top 5 groups of genes, which are differentially regulated between BTSCs and NSCs. The x axis indicates number of genes. FDR (false discovery rate) ≤ 0.005.

(F) Western blot for GPD1 of NSCs and BTSCs showing high GPD1 expression in BTSCs compared to NSCs; NSC and BTSC numbers indicate cells isolated from independent animals.

(G) Immunofluorescence of GPD1 confirms that it is only expressed by BTSCs but not NSCs *in vitro*.

the neurogenic niche of the subventricular zone (SVZ). We identified many factors, which were differentially expressed from NSCs to BTSCs. Among these factors, glycerol-3-phosphate dehydrogenase 1 (GPD1) was found to be exclusively expressed in dormant BTSCs and was further validated as a promising therapeutic target *in vivo*. Our results reveal a novel aspect of molecular regulation of stemness in cancer cells and suggest that GPD1 may be used as a novel therapeutic target.

RESULTS

Ribosome Profiling and Transcriptome Analysis of BTSCs and NSCs Identify BTSC-Specific Molecular Programs

Ribosome profiling provides information about the identity of translated RNA and the translation efficiencies of open reading frames, which generally correlate well with proteomic results (Ingolia et al., 2009, 2014). As outlined in Figure 1A, we used NSCs

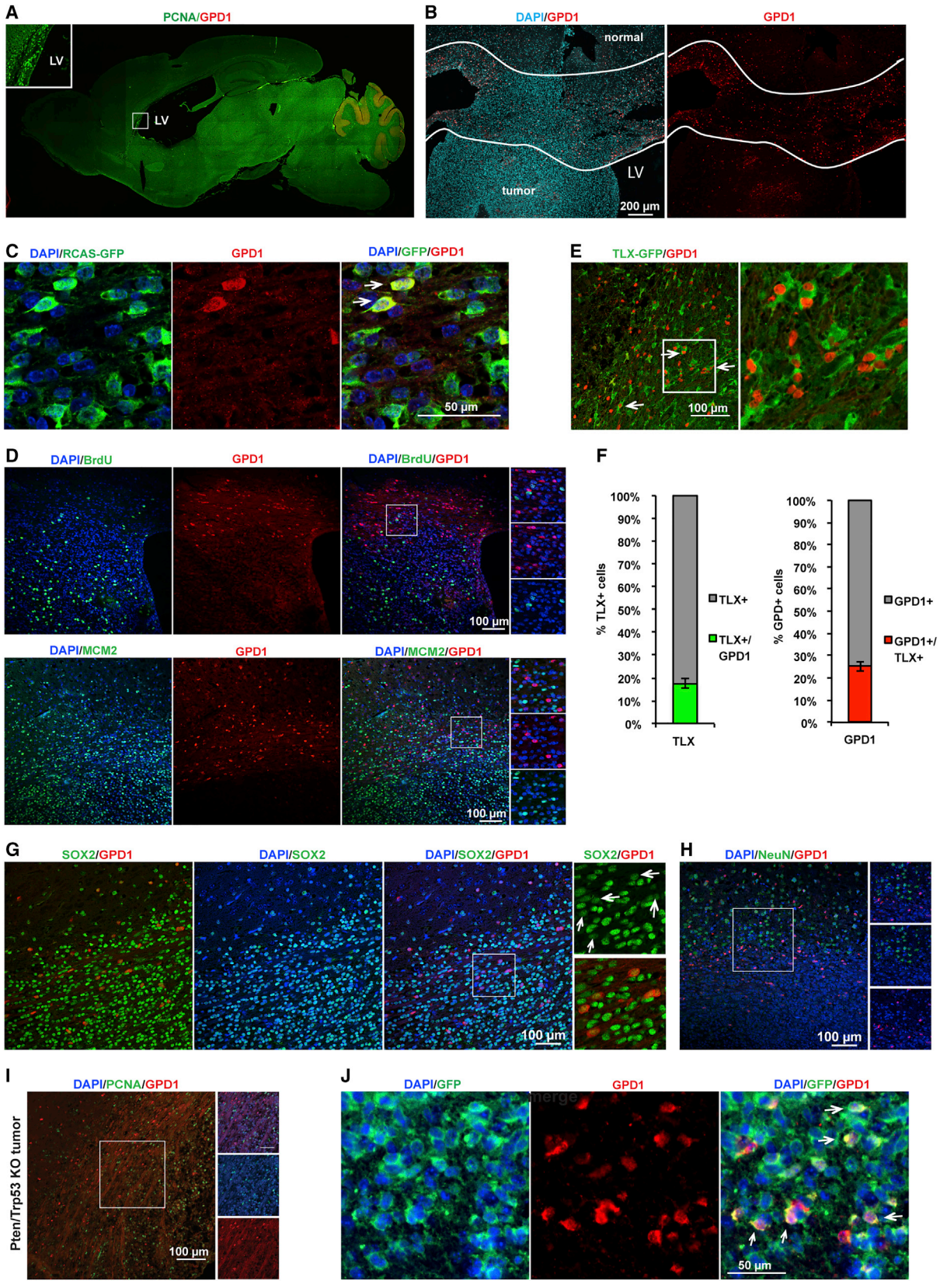

(legend on next page)

isolated from the adult SVZ, and BTSCs from glioblastoma induced with RCAS (Replication-Competent Avian sarcoma-leukosis virus long terminal repeat with Splice acceptor) retroviral vectors to drive PDGFB (platelet-derived growth factor subunit B) and AKT overexpression in Nestin-TVA (Ntv-a) mice, which carry the transgene expressing the receptor of avian leucosis virus subgroup A under the *Nestin* promoter (Holland, 2001; Zhu et al., 2014). We performed ribosome profiling and RNA sequencing (RNA-seq) in parallel using RNA isolated from the same cells and found that there is a rather small overlap between the ribosome profiling and the RNA-seq data in terms of differentially expressed genes between NSCs and BTSCs (Figure S1A). We next focused on the ribosome-profiling results, as the differentially translated RNAs identified in this experiment likely result in protein changes, which may serve as therapeutic targets (Table S1). Hierarchical clustering suggests that BTSCs have very specific molecular programs compared to NSCs (Figure 1B). Oxidation reduction and lipid metabolic processes are specifically upregulated in BTSCs (Figures 1C and 1D). GO (gene ontology) analysis further suggests molecular changes in cell adhesion, cell-cycle progression, and oxidation reduction process (Figure 1E). This suggests that there is a BTSC-specific molecular program, indicating a possibility to specifically target BTSCs without targeting NSCs.

To select specific candidates for further investigation, we used the following criteria: (1) the candidate should be a druggable target; (2) the candidate should be exclusively expressed by BTSCs but not NSCs; and (3) targeting the candidate should result in minimal toxicity or side effects. After candidate filtering with these criteria, GPD1 (glycerol-3-phosphate dehydrogenase 1) was selected for further investigation. First, we confirmed the ribosome profiling results by western blot analysis of different hits. Shown here are Anxa6 (Annexin A6, Figure S1B) and GPD1 (Figure 1F). For GPD1, we further performed immunofluorescence (IF) staining using the same cells and demonstrated that GPD1 is specifically expressed in BTSCs (Figure 1G). These data collectively confirm significant protein expression changes identified by ribosome profiling. GPD1 is important for the carbohydrate and lipid metabolism by catalyzing the reversible conversion of dihydroxyacetone phosphate (DHAP) and reduced nicotine adenine dinucleotide (NADH) to glycerol-3-phosphate (G3P) and NAD^+ (Figure S1C). GPD1 is highly expressed in liver, kidney, pancreas, adipose tissue, colon, and skeletal muscle. Nevertheless, *Gpd1*-null mutant mice had no abnormal phenotype, and germline mutations of *Gpd1* in humans only cause transient infantile hypertriglyceridemia that normalizes with age (Basel-Vanagaite et al., 2012; Prochazka et al., 1989). Due to these facts, GPD1 might be an attractive therapeutic target for glioblastoma treatment with very few side effects.

GPD1 Is Expressed in Infiltrating Dormant BTSCs

Little is known about the role of GPD1 in cancer. We first analyzed the expression of GPD1 in normal mouse brain and found that GPD1 is not expressed in the SVZ NSCs, which are positive for the cell proliferation marker PCNA (proliferating cell nuclear antigen) (Figure 2A, inset). The only cells expressing GPD1 in the mouse brain are the Bergman glia cells in the cerebellum (Figures 2A and S2A). Strikingly, GPD1-expressing cells in mouse glioblastoma are highly enriched around the border between tumor and normal brain tissue (Figure 2B). To further confirm that these cells are tumor cells, we used RCAS-GFP together with PDGFB and AKT to induce tumor formation, thus labeling tumor cells with a GFP reporter. We confirmed that $GPD1^+$ cells co-express GFP suggesting that they are indeed tumor cells *in vivo* (Figure 2C, arrows). We then performed a series of IF analysis using different molecular markers to determine the identity of the $GPD1^+$ cells *in vivo*. Bromodeoxyuridine (BrdU) pulse labeling (animals were sacrificed 2 h after injection) of tumor-bearing mice allows us to see proliferating tumor cells, and we found that $GPD1^+$ cells were negative for BrdU staining (Figure 2D). Additional staining of another cell proliferation marker MCM2 (minichromosome maintenance 2) further confirmed the same pattern, suggesting these cells are slow dividing cells (Figure 2D). Analysis of three individual slices of five tumors each (approximately 1,000 $GPD1^+$ cells counted per tumor) showed that less than 1% of cells were co-stained for GPD1 and a cell proliferation marker. The fact that we could hardly find any $GPD1^+$ cells positive for the above markers suggests that these are dormant cells *in vivo*. However, the expression of GPD1 *in vitro* is not restricted to dormant cells (Figures S2B and S2C), indicating this pattern is specifically found *in vivo*. Previously, we have shown that TLX^+ cells are BTSCs *in vivo* using Ntv-a;TLX-GFP mice (Zhu et al., 2014). In the Ntv-a;TLX-GFP tumor-bearing mice, we found that a subset of $TLX\text{-}GFP^+$ cells express GPD1 and vice versa (Figures 2E and 2F). $GPD1^+$ cells express the neural stem or progenitor marker Olig2 and Nestin

Figure 2. GPD1 Is Expressed by Dormant BTSCs but Not by NSCs *In Vivo*

(A) Sagittal section of an adult mouse brain showing that GPD1 expression is not detected in the mouse brain except in the Bergmann glial cells in the cerebellum; inset shows PCNA staining of proliferating cells in the SVZ, which is negative for GPD1 expression. LV, lateral ventricle. The image was acquired under the Tile Scan mode of Zeiss LSM800, and the images were automatically stitched together.

(B) GPD1 staining of mouse glioblastoma. $GPD1^+$ cells are mostly distributed along the tumor border (between the lines) infiltrating the corpus callosum.

(C) GFP and GPD1 co-localization (arrows) in tumors induced with RCAS PDGFB/Akt/GFP shows that $GPD1^+$ cells are tumor cells.

(D) GPD1 and BrdU/MCM2 staining of mouse brain tumors shows that $GPD1^+$ cells do not divide as they do not incorporate BrdU, and they are negative for MCM2 expression. Animals were sacrificed for brain section preparation 2 h after injection of BrdU.

(E) GPD1 co-staining with TLX-GFP (arrows indicate double-positive cells) in brain tumors obtained from TLX-GFP;Ntv-a mice.

(F) Quantification of TLX-GFP and GPD1 co-localization in brain tumors (n = 5). Graphs indicate mean ± SEM.

(G) GDP1 and SOX2 double staining in brain tumor sections. Note that $GPD1^+$ cells express low levels of SOX2 (inset, arrows).

(H) GPD1 and NeuN double staining shows that $GPD1^+$ cells are not differentiated neurons.

(I) In another tumor model that is induced with PTEN and p53 KO, GPD1 is also negative for proliferation markers (PCNA) and distributed at the tumor margin.

(J) PTEN/p53 KO BTSCs were transduced with GFP and xenografted to WT mice brains. Staining with anti-GFP and anti-GPD1 antibodies confirms that GPD1 cells are indeed tumors cells (arrows indicate double-positive cells).

$n \geq 5$ for all stainings, 1,000 cells counted per tumor.

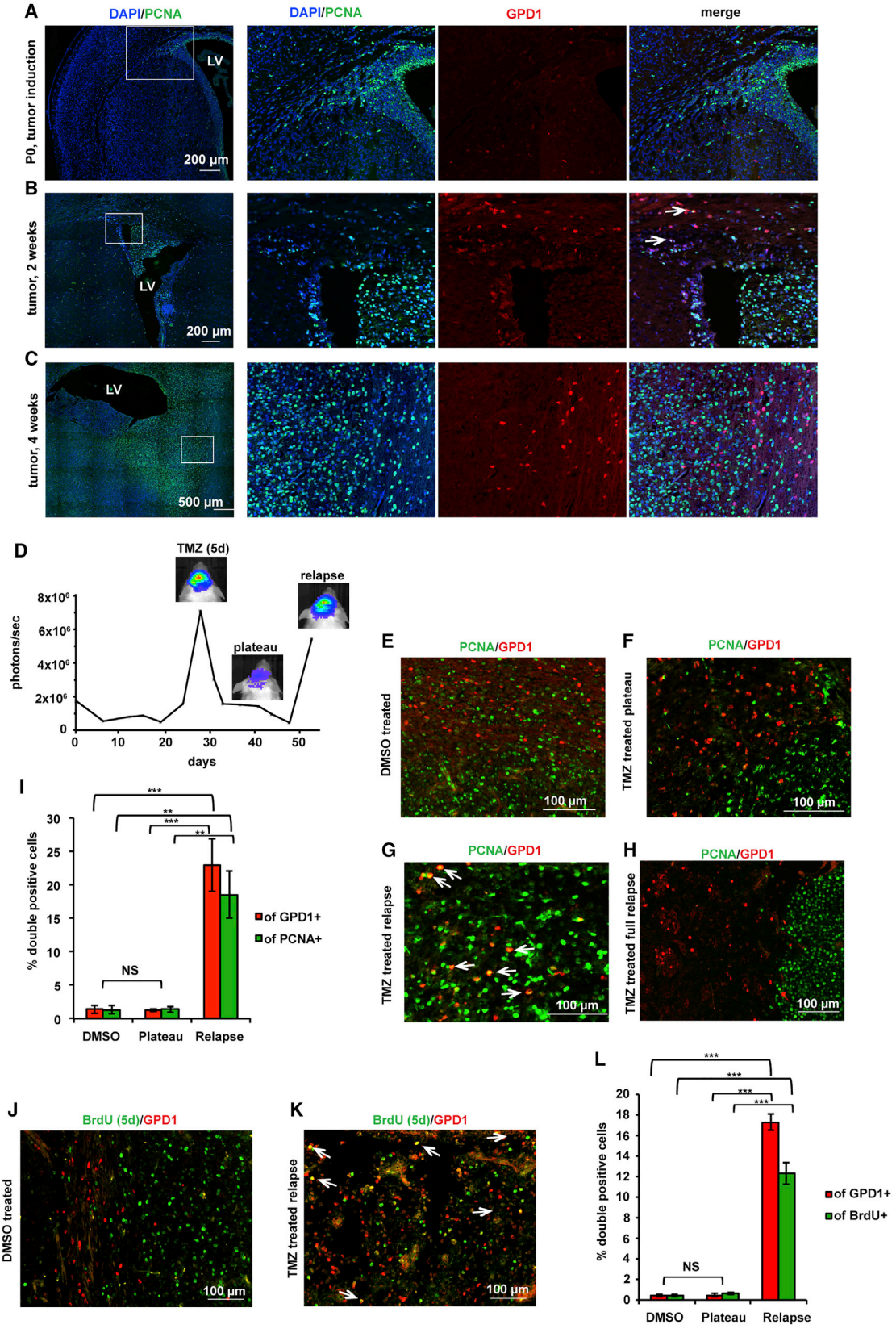

(legend on next page)

(Figures S2D and S2E) and express low levels of neural progenitor marker SOX2 (Figure 2G) but not the neuronal differentiation marker NeuN and DCX (Figure 2H; Figure S2F). We did not see a correlation between GPD1$^+$ cells and CD34$^+$ endothelial cells (Figure S2G), which implies that GPD1$^+$ cells are not preferentially localized to a vascular niche.

Additionally, we also confirmed the expression of GPD1 in PCNA$^-$ dormant cells in an independent mouse brain tumor model based on NSC-specific inactivation of *Pten* and *Trp53* (Pten;Trp53$^{Tlx\text{-}CreERT2}$) (Figure 2I) (Costa, 2019; Peterziel et al., 2012). As in the PDGF/AKT tumor model, GPD1 was also found at the tumor border (Figure S2H), and less than 1% of GPD1 cells were dividing (five individual tumors where analyzed as described above). To confirm that these GPD1$^+$ cells were tumor cells, tumors were dissected and the cells were cultured as BTSCs. After transduction with GFP, cells were sorted by fluorescence-activated cell sorting (FACS) and transplanted into brains of wild-type (WT) mice. These mice were sacrificed once they showed symptoms, and the brain slices were stained for GFP and GPD1. As GPD1$^+$ cells were also GFP positive (Figure 2J), thus confirming that GPD1$^+$ cells are indeed tumor cells also in this mouse brain tumor model. These results suggest that GPD1 expression identifies a dormant BTSC population *in vivo* and that these cells are highly enriched around the border of tumors.

GPD1 Expression Is Activated in Early Tumor Development and GPD1$^+$ Cells Exit Dormancy during Tumor Relapse after Chemotherapy

Since GPD1 is not expressed in NSCs in the SVZ, we set out to identify at what stage GPD1 expression starts during tumor initiation. While no expression of GPD1 could be observed in non-induced new-born control mice in the SVZ (Figure 3A), expression of GPD1 occurred in tumor lesions already 2 weeks after tumor induction. We frequently observed an enriched expression in the corpus callosum during early development of tumors (Figure 3B). In human glioblastoma, it is known that the corpus callosum is one of the mostly used migration routes of tumor cells (Demuth and Berens, 2004). Interestingly, we found some GPD1$^+$ cells to express PCNA (Figure 3B, arrows), which we rarely observed in fully developed brain tumors, suggesting that GPD1$^+$ cells have the potential to proliferate during tumor initiation. The distribution of GPD1$^+$ cells at the tumor border was observed 4 weeks after tumor induction and they are PCNA$^-$ cells (Figure 3C). This is consistent with the observation of preferential distribution of GPD1$^+$ cells at the tumor border at later stages. These results suggest that GPD1$^+$ cells are migratory BTSCs with the potential to proliferate during early initiation of tumors and they become dormant after tumor establishment.

It has been reported that BTSCs are resistant to TMZ therapy *in vivo* (Chen et al., 2012; Zhu et al., 2014). As the dormant phenotype of GPD1$^+$ cells suggests that they are TMZ-resistant cells, we applied TMZ treatment to tumor-bearing Ntv-a mice and collected tumor sections at different stages after TMZ treatment. A luciferase reporter was included for the tumor induction and allowed us to visualize tumor growth and response to TMZ treatment *in vivo*. The mice received the TMZ treatment for 5 days once their tumors reached a certain threshold. We sacrificed the animals at different time points: when the tumor reached a bottom plateau and did not shrink further, when it started to relapse, and when it had fully relapsed (Figure 3D; Figures S3A–S3D). Interestingly, co-staining of GPD1 with PCNA showed that GPD1$^+$ cells stayed dormant during the treatment (Figures 3F; Figure S3E) but started to divide when we observed tumor relapse with the luciferase imaging (Figures 3G, 3I, and S3E). Approximately 22% of all counted GPD1 cells were dividing cells, while around 18% of all PCNA$^+$ cells were GPD1$^+$. Once the tumor was fully relapsed, the number of dividing GPD1$^+$ cells decreased again indicating that they turned back to dormant cells (Figures 3H). To further analyze the proliferation ability of GPD1$^+$ cells, we conducted short-term BrdU labeling, by injecting BrdU 2 h prior sacrifice. With this method, however, we only stained few of the proliferating cells compared to PCNA staining and could not detect a significant increase in BrdU$^+$ GPD1-expressing cells (Figures S3F and S3G). To label more cells with BrdU, we injected BrdU for 5 consecutive days before sacrificing the mice and analyzing the proliferation pattern (scheme in Figure S3H). The labeling of dividing cells with BrdU showed that 17% of all GPD1$^+$ cells were also positive for BrdU and 12% of the BrdU population also expressed GPD1 and the time point of tumor relapse (Figures 3J–3L and S3I).

Figure 3. GPD1$^+$ Cells Appear during Tumor Initiation and Proliferate during Tumor Relapse

(A) Coronal section of newborn (P0) mouse brain, the time point when tumors were induced. While there is a lot of cell proliferation present in the SVZ, no GPD1 staining could be detected.

(B) GPD1 expression was observed in tumor lesions 2 weeks after tumors induction. Arrows indicates some GPD1 and PCNA double-positive cells, which suggests the GPD1 cells may proliferate during tumor initiation.

(C) After 4 weeks, once the tumor has grown substantially, GPD1 can be detected around the border of the tumor bulk, which consist mainly of fast dividing PCNA$^+$ cells. The image was acquired under the Tile Scan mode of Zeiss LSM800, and the images were automatically stitched together

(D) Experimental overview of analyzing GPD1 expression during TMZ treatment and tumor relapse.

(E) Coronal section of mouse treated with DMSO (control). GPD1$^+$ cells are not PCNA$^+$ tumor cells.

(F) GPD1 and PCNA staining of mouse brain tumors after TMZ treatment when it reached a bottom plateau; GPD1$^+$ cells are not affected but remain to be PCNA negative, although there are much fewer PCNA$^+$ cells as the tumor size decreased.

(G) GDP1$^+$ cells start to divide when a brain tumor relapses after chemotherapy, showing co-expression of GPD1 and PCNA (arrows).

(H) Once the tumor is fully relapsed, GPD$^+$ cells become negative for PCNA expression.

(I) Quantification of PCNA/GPD1 double-positive cells before and after TMZ treatment.

(J and K) Mice were injected with BrdU for 5 consecutive days before sacrifice. Pictures show GPD1 and BrdU co-stainings of DMSO-treated mice (J) and of TMZ-treated mice (K) once the tumor starts to relapse.

(L) Quantification of BrdU/GPD1 double-positive cells before and after TMZ treatment.

In (J), graphs indicate mean ± SEM, $n \geq 5$, $^{**}p < 0.01$, $^{***}p < 0.001$. Images in (E)–(K) were acquired under the Tile Scan mode of Zeiss LSM800 and areas of interest were shown as representative images.

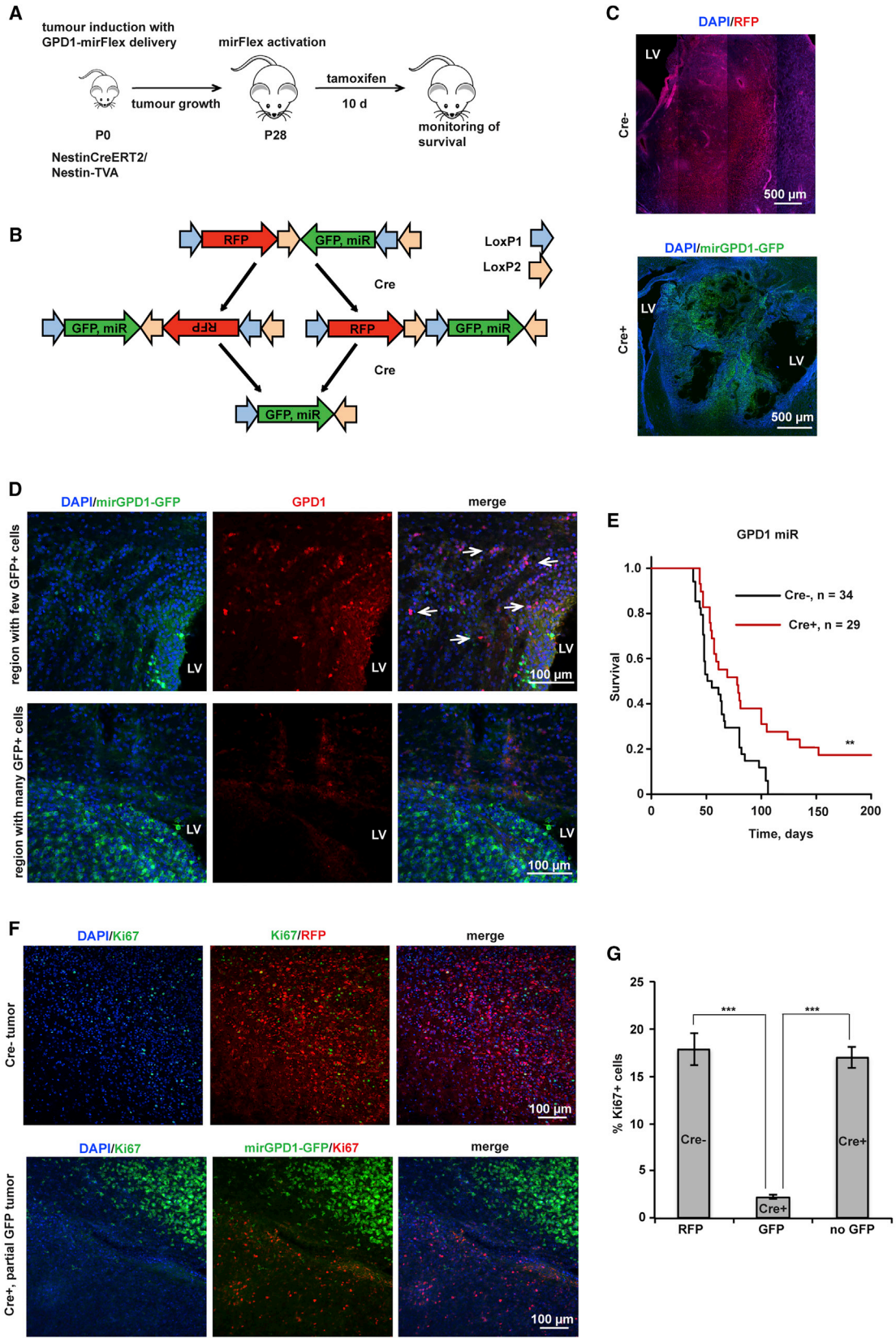

(legend on next page)

These results clearly demonstrate that GPD1$^+$cells are involved in tumor initiation, migration, and tumor relapse, whereas they become dormant when the tumor is fully developed or relapsed.

GPD1 Inhibition in Brain Tumors Leads to Prolonged Animal Survival

Next, we decided to investigate the function of GPD1 in brain tumors *in vivo*. We developed an inducible knockdown (KD) system, which allows the controlled expression of a target-specific microRNA in a Cre-dependent manner (Koo et al., 2011) (miRFlex, Figures 4A and 4B). We also incorporated a reporter conversion to monitor the induction of the Cre-mediated KD. Tumor cells switch the expression of RFP into GFP upon Cre activation (Figures 4B and 4C). We selected a microRNA, which efficiently blocks the expression of GPD1 in cell culture (Figures S4A and S4B; Table S4). It is important to note that the penetration of the KD construct is not always 100% in all the tumors, which enabled us to perform a mosaic analysis in some tumors harboring both green clones and clones that did not get the microRNA construct. Upon tamoxifen injection, after the tumor is fully developed (P28), we confirmed by IF that GPD1 was efficiently downregulated in green tumor cells, while it was expressed in tumor cells that did not have the microRNA (Figure 4D). Kaplan-Meier survival analysis demonstrates that the KD of GPD1 results in a significantly prolonged survival of tumor-bearing animals (median survival 53 versus 78 days), whereas mice obtaining a control scrambled miRNA had no survival benefit (Figure 4E; Figure S4C). Treatment with TMZ also lead to a similar increase of the median survival as GPD1 KD. However, while TMZ treatment lead to a longer survival of mice with early symptoms, GPD1 KD had a bigger effect on long-term survival. A combined therapy resulted in an increase of both survival of mice with early-onset symptoms and long-term survival. While the three treated groups were not significantly different from each other, the median survival for the group with both treatments was increased (78 days versus 85 days) (Figure S4D).

For further investigation of the survival phenotype, we analyzed tumors that were only partially labeled with the KD reporter construct, which allows a mosaic analysis of GPD1 KD cells (GFP$^+$) and control tumor cells (GFP$^-$) from the same tumor. While the GFP$^+$ cells in those tumors showed dramatically decreased proliferation as shown by co-staining with Ki67 and GFP, the GFP$^-$ cells had similar proliferation rates as the RFP$^+$ tumors (Figures 4F and 4G). It is intriguing that blockade of GPD1 results in a decrease of tumor cell proliferation, although GPD1 expression is restricted to the dormant BTSCs. These results suggest that dormant BTSCs indeed contribute to tumor growth. We conclude that inhibition of GPD1 *in vivo* attenuates tumor growth and results in prolonged animal survival, demonstrating that GPD1 is a valid therapeutic target in glioblastoma *in vivo*.

Loss of GPD1 Impairs Multiple Pathways Important for BTSCs Maintenance

The molecular mechanism involving GPD1 has been mostly studied in yeast, in which GPD1 expression is considered as a reporter for osmotic stress signaling (Akhtar et al., 2000). To explore the molecular consequences after loss of GPD1 in BTSCs, we used CRISPR/Cas9 to knock out (KO) GPD1 in mouse BTSCs *in vitro* (Figures S5A and S5B) and performed RNA-seq analysis of these cells (Table S2). GO analysis indicates that the significantly changed genes are involved in protein translation, cell proliferation and differentiation, and cell adhesion pathways (Figure S5C). Among these changes, there are many important regulators for NSCs or BTSCs, e.g., *Tlx (Nr2e1)*, *Nestin (Nes)*, *CD44*, *Gap43*, *Met*, and *Hmga1/2* are downregulated suggesting an impaired stem cell activity in *Gpd1* KO cells (Figure 5A) (Nishino et al., 2008; Osswald et al., 2015; Pietras et al., 2014; Zhong et al., 2016; Zhu et al., 2014). Genes that are important for neuronal differentiation such as *Dlx1/2/4*, *Prox1*, *Sox4*, *Chd7*, *Dcx*, *Tet1/2*, and *Rdh10/14* are upregulated suggesting induction of neuronal differentiation in *Gpd1* KO BTSCs (Figure 5A) (Bergsland et al., 2006; Cimmino et al., 2011; Dyer et al., 2003; Feng et al., 2013). Genes promoting cell-cycle progression (including *Ccnd1/2*, *Mcm2/4/5/6/7/8*, *Ccne1*, and *Ccna1*) are downregulated, and tumor suppressor genes (including *Ptch1*, *Foxo3/4*, *Nf1*) are upregulated as well as genes that are important for regulating autophagy (including *Atg7/10/13/14*) suggesting growth inhibition of tumors after loss of *Gpd1* (Figure 5A). Annexins, a family of proteins that can bind to certain membrane phospholipids in a Ca^{2+}-dependent manner (Gerke et al., 2005), are downregulated (including *Anxa1/2/3*) in the *Gpd1* KO cells (Figure 5A). This suggests loss of GPD1 may affect additional signaling transduction pathways. Gene set enrichment analysis (GSEA) also suggests that *Gpd1* KO cells have a decreased expression of genes that are downregulated in the *Tlx* KO stem cells (Zhang et al., 2008), as well as of genes that are essential for epithelial mesenchymal transition (Figures 5B and 5C), suggesting an impaired stem cell identity. To functionally validate the *Gpd1* KO phenotype, we performed a differentiation assay by withdrawing growth factors from the culture medium, which led to an increase of neuronal differentiation and a decrease of oligodendrocyte differentiation suggesting loss of GPD1 restores the neuronal differentiation potential of BTSCs (Figures 5D, 5E, S5D, and S5E show BTSCs from another mouse treated the same way).

Figure 4. GPD1 Inhibition Results in Prolonged Survival of Tumor-Bearing Mice

(A and B) Graphic description of the experiment design (A) and the inducible *in vivo* KD system (B, mirFlex).

(C) Tamoxifen injection leads to expression of mirGPD1-GFP in Cre$^+$ tumor-bearing mice but not the Cre$^-$ tumors, which maintain RFP expression. The images were acquired under the Tile Scan mode of Zeiss LSM800, and the images were automatically stitched together

(D) Tumor cells express GFP, which indicates the mirGPD1 expression, are negative for GPD1 expression suggesting effective KD of GPD1 expression *in vivo*. Top panel shows GPD1 expression in a control area with few GFP cells.

(E) GPD1-inducible KD in fully established mouse tumors leads to a prolonged survival, $p = 0.004$.

(F) GPD1 inhibition results in decrease of tumor cell proliferation *in vivo*. Tumors have a mosaic induction of GPD1 KD were selected for Ki67 staining.

(G) Ki67 proliferation index in RFP or GFP or Cre$^-$ tumor cells represent WT or GPD KD cells, respectively. The graph indicates mean ± SEM, $n \geq 5$, $p \leq 0.0005$.

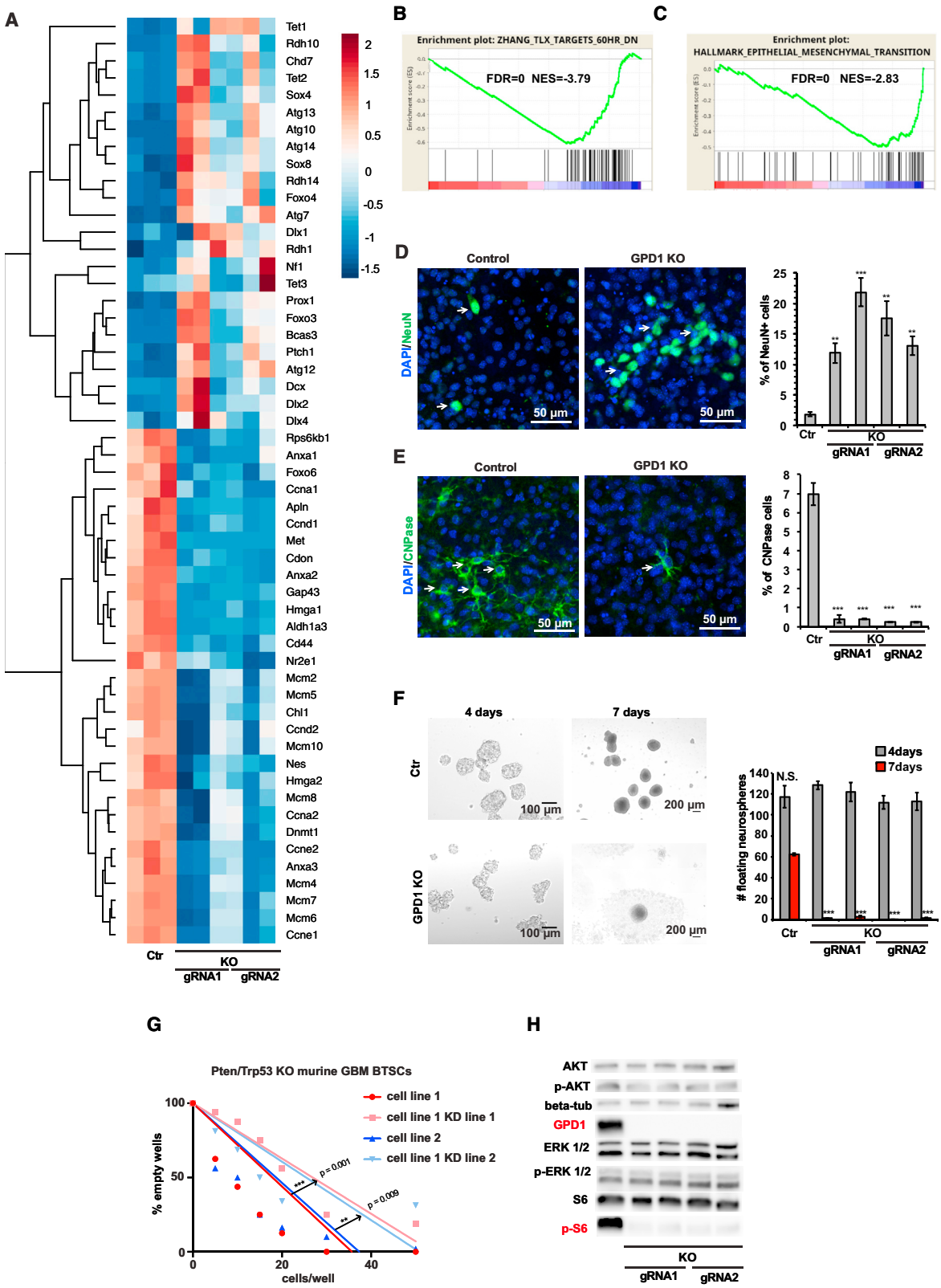

Figure 5. Loss of GPD1 Induces Molecular Changes that Disrupt BTSC Maintenance

(A) Heatmap analysis shows changes of genes that are important for regulation of stem cell features in GPD1 KO BTSCs. RNA-seq was performed using GPD1 KO BTSCs. GPD1 KO was performed using CRISPR/CAS9; KO cells obtained based on 2 different sgRNAs were used as shown by gRNA1 and gRNA2.

(legend continued on next page)

We also performed a tumorsphere-forming assay, which reflects the self-renewal capacity of BTSCs *in vitro*. We observed that most of the *Gpd1* KO tumorspheres spontaneously attach to culture plates, which suggests a spontaneous differentiation phenotype (Figures 5F; Figure S5F). We also confirmed that by KD of *Gpd1* in *Pten/Trp53* KO BTSCs. The limiting dilution assay clearly demonstrated loss of stem cell activity upon inhibition of GPD1 (Figure 5G).

We also observed downregulation of key regulators of the mTOR (mechanistic target of rapamycin) pathway such as ribosomal protein S6 kinase B1 (*Rps6kb1*) (Figure 5A), which suggests an inhibition of mTOR activity. This was further supported by a significant downregulation of phosphorylated S6 (p-S6) but not of phosphorylated Akt (p-Akt) in the *Gpd1* KO BTSCs (Figures 5H and S5G), suggesting a rather specific inhibition of p-S6 upon loss of GPD1. We observed that GPD1$^+$ cells are also positive for p-S6 *in vivo* (Figure S5H, arrows), indicating that mTOR activity is active in these dormant GPD1$^+$ cells. Interestingly, the phospholipid pathway was shown to be able to activate the mTOR pathway (Foster, 2013), which suggests that the mTOR pathway may act downstream to GPD1 in these dormant BTSCs. mTOR is known to be essential for protein translation, and we confirmed that the gene sets that are downregulated in the *Gpd1* KO BTSCs are highly enriched for E2F, MYC targets, and ribosome biogenesis genes (Figures S5I, S5J, and S5K), which are known to be positive regulators of protein synthesis. Since GPD1 is important for the regulation of lipid metabolism, we found that expression of many genes affecting the glycerophospholipid metabolism are altered in the *Gpd1* KO BTSCs (Figure S5L). These results suggest that a profound change for BTSCs survival and maintenance occurs in the *Gpd1* KO cells, demonstrating that GPD1 is essential for the maintenance of BTSCs.

A Metabolomics Assay Reveals the Essential Role of GPD1 in Regulating Metabolism in BTSCs

GPD1 is a metabolic regulator, and the role of GPD1 suggests that BTSCs have a distinct metabolic status compared to NSCs. To systematically analyze the metabolic relevance of GPD1 in BTSCs, we performed metabolomic and lipidomic analysis using the same cells as for the ribosome profiling experiment and the *Gpd1* KO cell lines deriving from these BTSCs. From this experiment, we found that indeed the BTSCs have a very different metabolomic profile from NSCs (Table S3). Principal-component analysis (PCA) based on lipid analysis and metabolite analysis show that BTSCs are distinct from NSCs (Figures 6A–6C), whereas *Gpd1* KO in BTSCs leads to a dramatic change in both analyses (Figures 6A–6C). The significantly changed lipid species were subjected for KEGG (Kyoto Encyclopedia of Genes and Genomes) pathway analysis, and we found that the most significantly changed lipid pathway is glycerophospholipid metabolism, which is strongly supporting the role of GPD1 in BTSCs because the role of GPD1 is to mediate the generation of glycerol-3-phosphate, which is a precursor for glycerophospholipid metabolism. Further analysis demonstrates changes of specific lipid species, i.e., phosphatidylethanolamine (PE) and phosphatidylcholine (PC), and inhibition of GPD1 reverses the changes of several PEs and PCs between NSCs and BTSCs (Figures 6E and 6F). From the metabolomic assay, we found that several pathways are significantly enriched (Figure 6G). The most notable pathway is the taurine and hypotaurine pathway (Figures 6G, 6H, and S6A–S6C). This pathway is upregulated in BTSCs in comparison to NSCs and is downregulated in Gpd1 KO BTSCs. It is known that this pathway is essential for stress response in cells (Aruoma et al., 1988). Taurine is known to be protective during osmotic stress in cells, and hypotaurine is protective during oxidative stress (Aruoma et al., 1988; Hussy et al., 1997). This is in line with the known function of *Gpd1* as a stress-response gene in yeast, particularly for osmotic stress. These results demonstrate BTSCs have a distinct metabolic status, which is dependent of GPD1 expression.

GPD1 Is Expressed in Multiple Human Cancers, and the Expression Is Enriched at the Tumor Border in Human Glioblastoma

Furthermore, we analyzed GPD1 expression in human cancers. We used the cancer genome atlas (TCGA) database and found that GPD1 is expressed in human glioblastoma and high expression correlates with worse prognosis, including both overall survival and progression-free survival (Figure 7A). A survival benefit could also be observed in glioma patients with a low GPD1 expression from an independent cohort of patients (Gravendeel et al., 2009) (Figure S7A). Importantly, GPD1 overexpression was observed in multiple cancer entities (Figure 7B). Together these data show that GPD1 is expressed throughout different cancer types with glioblastoma and glioma having the highest expressions after renal cell carcinoma (RCC) and liver cancer. The high expression of GPD1 is also correlated with a worse survival in RCC (Figure S7B). We did not observe a major difference in GPD1 expression in different glioblastoma subgroups (proneural, classic, and mesenchymal) (Phillips et al., 2006; Verhaak et al., 2010) (Figure S7C). It is important to note that we found markers that represent different subgroups to be affected in the *Gpd1* KO BTSCs, e.g., *Dcx*, *Sox4* for proneural, *Ccnd2* and *Nes* for classic, and *CD44* for mesenchymal. This suggests that there is a general principle in terms of expression and function of GPD1 across different subgroups. Using the Human Protein Atlas database (https://www.proteinatlas.org/), we found that GPD1 is heterogeneously expressed in human glioblastoma (Figure S7D). To better characterize the GPD1$^+$ cells in human

(B and C) GSEA of differentially changed genes in GPD1 KO shows downregulation of the Tlx-dependent molecular network (B) and genes that are involved in the epithelial-mesenchymal transition (EMT; C), which suggests impairment of stem cell molecular signatures.
(D and E) Induction of differentiation was performed by culture BTSCs without EGF and half the amount of FGF2 compared to normal culture conditions. GPD1 KO BTSCs preferentially differentiate into NeuN$^+$ neurons (D), and the potential to differentiate into oligodendrocyte is impaired (E) ($n \geq 4$, $^{**}p < 0.01$, $^{***}p < 0.001$).
(F) Tumorspheres of GPD1 KO BTSCs spontaneously attach to the plate; the results were obtained from 2 different time points ($n \geq 4$, $p \leq 0.0001$ for all cell lines).
(G) Limiting dilution assay shows GPD1 KD leads to reduced stem cell frequency in PTEN/p53 KO mouse BTSCs.
(H) Western blot analysis of GPD1 KO BTSCs demonstrates that loss of GPD1 leads to a striking reduction of p-S6, without affecting p-AKT or p-ERK level.
Graphs indicate mean ± SEM.

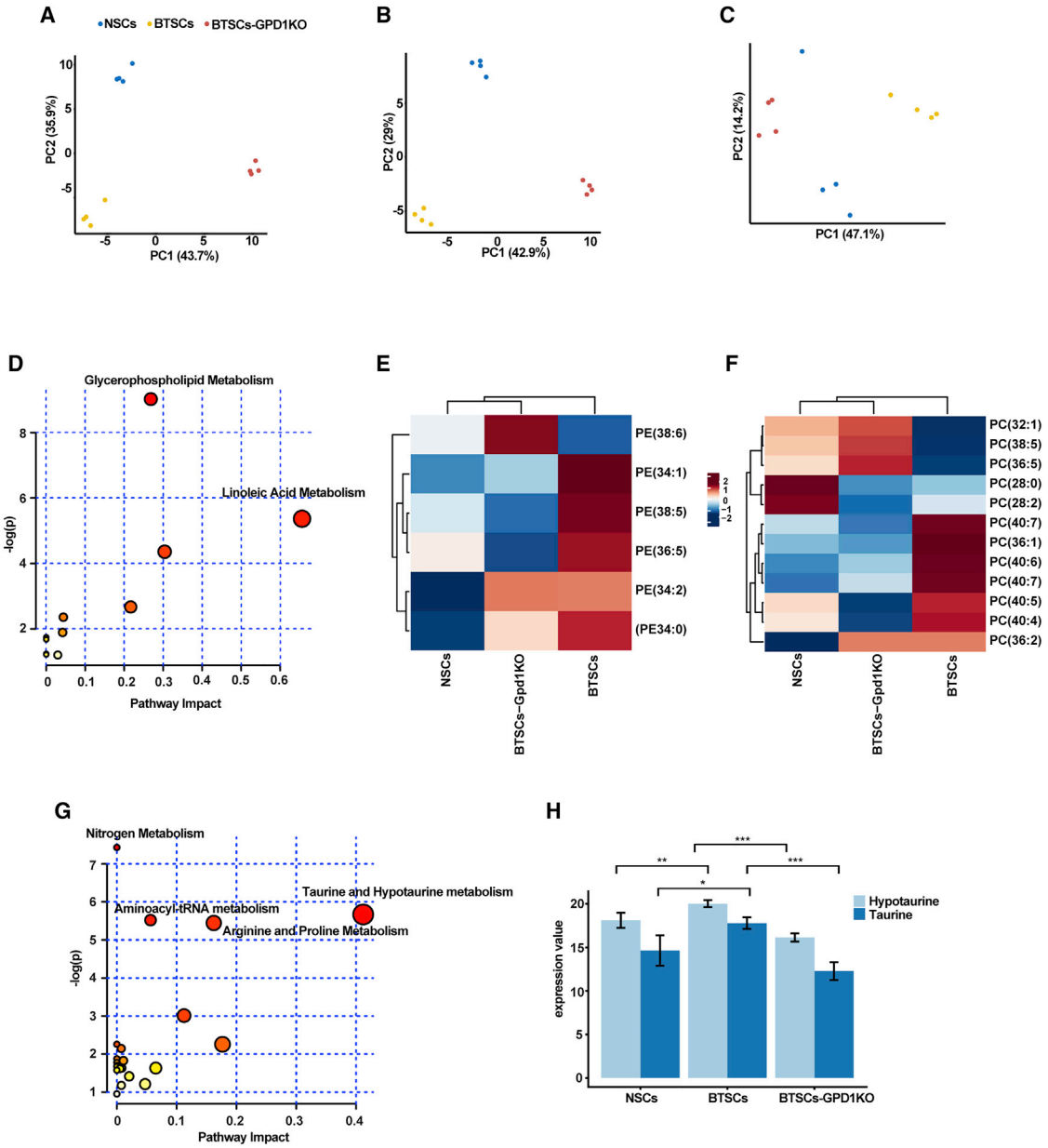

Figure 6. GPD1 Is Essential for the Maintenance of Metabolic Signature in BTSCs

(A) Lipid species of NSCs, BTSCs, and BTSCs-Gpd1KO detected in positive ionization mode were subjected for PCA analysis.

(B) Lipid species of NSCs, BTSCs, and BTSCs-Gpd1KO detected in negative ionization mode were subjected for PCA analysis. Note that NSCs and BTSCs are very distinct from each other, and GPD1 KO dramatically shifts the lipidome of BTSCs.

(C) PCA projection of metabolomic results demonstrate GPD1 KOs were shifted toward NSCs in comparison to the BTSCs. Note that there is a greater heterogeneity observed between samples, which was not seen in the lipidomic experiment using the same cells.

(D) Scatterplot of enriched KEGG pathways in lipidomic experiment when comparing NSCs with BTSCs. Color shift indicates level of significance; size of dots correlates with the number of lipid species. Note that the most significantly changed pathway is the glycerophosphlipid pathway, which is controlled by GPD1. Significant pathways are labeled ($p \leq 0.005$).

(E) Several phosphatidylethanolamines (PEs) were significantly changed in BTSCs, but the changes were reversed in GPD1 KO BTSCs.

(F) Similar to the PEs, significantly changed phosphatidylcholines (PCs) were also reversed upon GPD1 KO.

(G) Scatterplot of enriched KEGG pathways in the metabolomic assay comparing NSCs and BTSCs. Significant pathways are labeled ($p \leq 0.005$). Note that the taurine and hypotaurine pathway is significantly changed.

(H) Hypotaurine and taurine expression levels are increased in in BTSCs but decreased in BTSCs-Gpd1 KO.

Graphs indicate mean ± SEM, $^{**}p < 0.01$, $^{***}p < 0.001$.

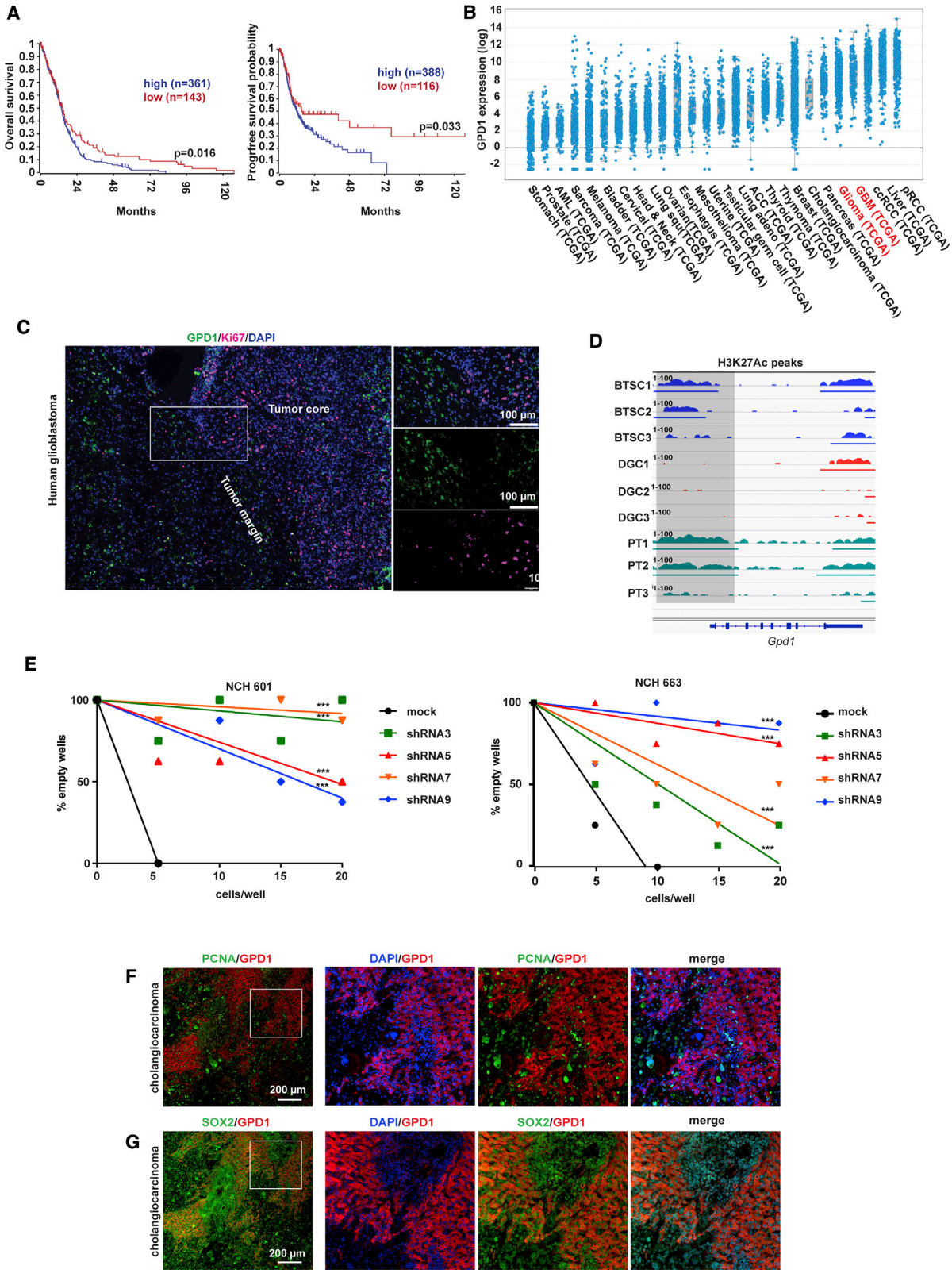

(legend on next page)

glioblastoma, we selected human tumor sections including the tumor margin characterized by a lower cell density. Ki67 staining indicates the proliferative tumor core, whereas the GPD1$^+$ cells are enriched at the tumor border, and they are negative for Ki67 expression (Figure 7C). We also analyzed GPD1 expression in published human brain tumor single-cell RNA-seq results (Darmanis et al., 2017; Patel et al., 2014; Tirosh et al., 2016; Venteicher et al., 2017). We only found reasonable numbers (550 and 490, respectively) of *Gpd1*-expressing cells in two studies (Tirosh et al., 2016; Venteicher et al., 2017). We applied correlation analysis to find genes co-expressed with *Gpd1*, and DAVID analysis was used to find the enriched GO terms in these genes. As shown in Figure S7E, we observed enrichment on genes regulating protein folding and cell adhesion, which suggests that the GPD1 positive cells are migrating cells and are active in stress response. This is consistent with the feature of GPD1 cells we observed in our mouse model. To further analyze the expression of GPD1 in human glioblastoma, we analyzed the H3K27ac chromatin immunoprecipitation sequencing (ChIP-seq) results of BTSCs and differentiated glioblastoma cells (DGCs) from human patients (Suvà et al., 2014). H3K27ac marks promoters and enhancers of actively transcribed genes. We found that the *Gpd1* promoter area is flanked by H2K27Ac peaks in BTSCs and patient tissues (PTs) but not in DGCs (Figure 7D), suggesting the GPD1-expressing cells in human glioblastoma are also BTSCs. Consistent with the mouse brain tumor results, the human tumor results suggest that GPD1 is an indicator for dormant BTSCs and a candidate therapeutic target in human brain tumors.

To investigate whether human glioblastoma stem cells also require GPD1 expression for their maintenance, we first found that GPD1 is also expressed in multiple human BTSCs (Figure S7F). Two cell lines, NCH601 and NCH663, were used for short hairpin RNA (shRNA)-mediated *Gpd1* KD (Figure S7G), and a limiting dilution assay was performed. We observed strong reduction of tumorsphere formation frequency in all the *Gpd1* KD cells (Figures 7E). After 2 weeks, fewer wells showed tumorsphere growth, and the tumorspheres were much smaller (Figure S7H).

Since GPD1 is expressed in other tumors, this raises the question of whether GPD1 is also expressed in slow dividing tumor cells. We first analyzed general correlation between GPD1 and PCNA or Ki67 in the R2 database (https://hgserver1.amc.nl:443/); we found that the expression of GPD1 is negatively correlated with PCNA and Ki67 (Figure S7I). We then analyzed GPD1 expression in mouse hepatocellular carcinoma, cholangiocarcinoma, and skin cancers. Interestingly, we found that GPD1$^+$ cells are PCNA$^-$ but are positive for a stem cell marker SOX2 (Figures 7F and 7G). However, we also found that GPD1 is downregulated in mouse hepatocellular carcinoma (Figure S7J), and we could not detect expression of GPD1 in skin tumors (data not shown). Therefore, whether GPD1 plays a similar role in other tumor entities need to be carefully analyzed case by case.

DISCUSSION

In this study, we identified that GPD1 is expressed by dormant BTSCs but not by NSCs *in vivo* and that its expression is essential for BTSC maintenance. Loss of GPD1 leads to impaired BTSC maintenance pathways, which results in prolonged animal survival. This functionally validates GPD1 as a therapeutic target for treatment of glioblastoma. The association between GPD1 expression and BTSC dormancy sheds new light on the molecular regulation of CSC dormancy.

CSCs are a key target for cancer therapy, but many of the already proposed protein targets are often important for normal stem cells and their development. For instance, Bmi1 is important for CSCs but also for normal stem cell self-renewal (Park et al., 2004). Nuclear receptor TLX is expressed only in the brain, implying fewer side effects are expected at the periphery by targeting TLX (Zhu et al., 2014), but TLX is also essential for brain development and NSC maintenance (Wang et al., 2013). This indicates that CSCs hijack stem cell pathways of normal stem cells and conversely suggests that they may acquire unique signatures for regulating "cancer stemness." Here, by applying a comprehensive RNA-seq, ribosome profiling, and metabolomic experiment comparing NSCs and BTSCs, we unravel unique molecular changes in the BTSCs, which can be further explored to find additional therapeutic targets without harming NSCs.

The finding that GPD1 is expressed only in the dormant BTSCs is surprising as we performed the screen using proliferating BTSCs *in vitro*. Analyzing expandable cells was necessary due to the large amounts of active ribosomes needed for the ribosome profiling experiments. GPD1 has been studied as an osmotic stress-responsive gene in yeast (Aiba et al., 1995; Albertyn et al., 1994). GPD1 expression is quickly induced upon osmotic stress, and high osmolarity glycerol (HOG1) mitogen-activated protein kinase is essential for the activation of the expression of GPD1 (Albertyn et al., 1994). The mammalian HOG1 homolog p38 was identified as a stress-responsive protein, and it was proposed to regulate stem cell quiescence or tumor dormancy (Sosa et al., 2014). However, we did not observe that p38 regulates GPD1 expression in BTSCs (data not shown). The upregulation of stress-response pathways (misfolded protein response, taurine and hypotaurine) in BTSCs

Figure 7. GPD1 Expression and Function in Human Glioblastoma and Other Tumor Entities

(A) Lower expression of GPD1 in human glioblastoma (TCGA database) correlates with better overall survival prognosis and with better progression-free survival.

(B) Analysis of GPD1 expression in different human cancers in the TCGA database. Glioblastoma and gliomas (red) have high expression of GPD1 among human cancers.

(C) GPD1 expression is distributed around the tumor border of human glioblastoma. Ki67 expression indicates tumor core. Inset shows that GPD1$^+$ cells are negative for Ki67 (5 individual tumors analyzed).

(D) H3K27Ac ChIP-seq analysis of human *Gpd1* locus in BTSCs, DGCs (differentiated glioblastoma cells), and PT (patient tissue). Gpd1 promoter area is flanked by H3K27Ac marks in BTSCs and PT but not in DGCs; this suggests that GPD1 is expressed in human BTSCs but not in differentiated tumor cells

(E) Limiting dilution assay of GPD1 KD in human primary BTSC NCH 663 and NCH 601. Note there is a dramatic loss of sphere-forming capacity in both cells upon GPD1 KD, which was performed using 4 independent shRNAs. $p < 0.001$ for all KD cell lines.

(F and G) GPD1 is expressed in mouse cholangiocarcinoma, and GPD1$^+$ cells are PCNA$^-$ (F) but Sox2$^+$ (G). 5 individual tumors were analyzed.

suggests that GPD1 upregulation is triggered by a stress pathway. As the GPD1 positive cells are at the invasion front of tumors, this means they are facing a changing environment during tumor progression. It is also known that human glioblastoma patients develop edema (Kaal and Vecht, 2004); therefore, a change of osmolarity in the brain is expected. Future experiments should try to determine the link between GPD1 and edema in glioblastoma.

GPD1 catalyzes the redox conversion of dihydroxyacetone phosphate to glycerol-3-phosphate, which can be further used to generate glycerol. This leads to rerouting of the energy flow from the glycolysis pathway, and active glycolysis is a signature of proliferating tumor cells. Intriguingly, an elevated glycerol level is associated with dormancy in insect development during diapause (Chino, 1957), which refers to dormancy induction of animal development upon environmental limitations. Increase of glycerol storage during diapause provides energy for diapause exit (Chino, 1957). Hibernating black bears switch off the glycolysis pathway but maintain an active glycerol metabolism pathway (Ahlquist et al., 1984). Therefore, an active glycerol metabolic process is likely a general signature for dormancy. It is fascinating that BTSCs may activate this environment-induced dormancy pathway to survive in a very challenging glioblastoma microenvironment, which is known to be hypoxic and which drastically promotes cell death. One additional consequence of enhanced glycerol levels in BTSCs is to generate phosphatidic acid, which is able to activate the mTOR pathway (Foster, 2013). This might be a specific mechanism of mTOR regulation of stress response in dormant CSCs. This possibility is supported by our finding that *Gpd1* KO cells greatly reduced the level of p-S6. One important result we showed here is that, although GPD1 expression is restricted to dormant BTSCs, inhibition of GPD1 in brain tumors leads to long-term decrease of cell proliferation *in vivo*. This suggests that the $GPD1^{+}$ dormant BTSCs contribute to brain tumor proliferation and maintenance, providing functional relevance for dormant CSCs as a therapeutic target. This also suggests the non-stem cells cannot self-renew *in vivo*, which is very similar to our previous finding that targeting *Tlx* in slow dividing BTSCs leads to decrease of tumor cell proliferation *in vivo* (Zhu et al., 2014). We also provide evidence showing that BTSCs upregulate the GPD1-dependent glycerophospholipid metabolism pathway and the taurine and hypotaurine pathway, which suggests that GPD1 expression on the one hand maintains lipid metabolism in BTSCs; on the other hand, GPD1 expression also makes the BTSCs become more resistant to stress.

An intriguing feature of GPD1 revealed here is that it is expressed only by BTSCs but not NSCs. This reduces the possible side effects when therapeutically targeting it in cancer patients. It is important to note that GPD1 KO mice are completely viable, and there are no major disease phenotypes observed (Prochazka et al., 1989). A biallelic mutation of GPD1 in human patients only results in a transient infantile hypertriglyceridemia phenotype (Basel-Vanagaite et al., 2012). This suggests that targeting GPD1 in human cancers will cause very few side effects. As the human GPD1 protein structure was solved with a well-defined substrate-biding domain (Ou et al., 2006), the druggability of GPD1 is likely to be very high. Thus, GPD1 is an attractive therapeutic target for glioblastoma.

STAR★METHODS

Detailed methods are provided in the online version of this paper and include the following:

- KEY RESOURCES TABLE
- LEAD CONTACT AND MATERIALS AVAILABILITY
- EXPERIMENTAL MODEL AND SUBJECT DETAILS
  - Mouse lines
  - Mouse housing
  - Tumor induction
  - Human samples
  - Cultivation of human glioma stem cells
  - Treatments of mice
  - Mouse cell lines
- METHOD DETAILS
  - Ribosome Profiling and mRNA sequencing
  - Cell culturing for metabol/lipid-omics experiments
  - LC-MS/MS experiments for metabolomics
  - LC-MS/MS experiments for lipidomics
  - Immunohistochemistry and Western Blots
  - Cell Culture Experiments
  - Lentiviral production and GPD1 shRNA knockdown in human glioma stem cells
  - Cloning and validation if GPD1 KD microRNA construct
  - Cultivation of pten/p53 knockout cell lines
  - Transfection of pten/p53 knockout cells
  - CRISPR /Cas9 mediated GPD1 KO in cultured BTSCs
- QUANTIFICATION AND STATISTICAL ANALYSIS
  - Ribosome profiling data analysis
  - RNA-seq data analysis
  - Immunohistochemistry
  - GPD1-KO survival analysis
  - Differentiation assay neurosphere assay
  - Limited dilution assay
  - Metabolomics/lipdiomics data analysis
  - Weighted Gene Coexpression Network Analysis (WGCNA) of Single-cell RNA-seq data
  - Murine tumor samples
- DATA AND CODE AVAILABILITY

SUPPLEMENTAL INFORMATION

Supplemental Information can be found online at https://doi.org/10.1016/j.stem.2019.06.004.

ACKNOWLEDGMENTS

We would like to thank the DKFZ preclinical center for assistance for animal experiments; the Imaging and Cytometry, Genomics and Proteomics Core Facilities of the DKFZ; and the Carl Zeiss Imaging Center in the DKFZ for their support. We thank Yue Zhuo for improving the graphic summary. This work was supported by the DKFZ and BayerHealthCare alliance (to H.-K.L. and P.R.), the Deutsche Krebshilfe (110226 to H.-K.L.), the German Research Foundation (DFG; SFB/TR209 to D.F.T. and P.A.), and the ERC (European Research Council) consolidator grant (647055) (to H.-K.L.)

AUTHOR CONTRIBUTIONS

Conceptualization, H.-K.L. and P.R.; Investigation, P.R., A.N., P.P., T.S.S., A.A.A., Y.W., M.S., S.D., and O.F.; Methodology, P.Z., K.D., and G.K.; Formal Analysis, P.R., C.S., P.P., and H.-K.Q.; Writing, H.-K.L. and P.R.; Resources,

B.R., C.H.-M., M.H., T.G., D.F.T., B.C., and P.A.; Review and Editing, H.-K.L., P.R., and C.S.; Visualization. P.R., H.-K.L., and C.S.; Funding Acquisition, H.-K.L., P.R., P.A., and B.R.; Project Administration, H.-K.L. and P.R.; Supervision, H.-K.L., P.R., P.A., B.B., and B.R.

DECLARATION OF INTERESTS

P.R. and H.-K.L. are inventors of a patent application related to this study, and this project is partially funded by BayerHealthCare through the DKFZ-BHC alliance.

Received: March 1, 2018
Revised: March 15, 2019
Accepted: June 7, 2019
Published: July 11, 2019

REFERENCES

Ahlquist, D.A., Nelson, R.A., Steiger, D.L., Jones, J.D., and Ellefson, R.D. (1984). Glycerol metabolism in the hibernating black bear. J. Comp. Physiol. B *155*, 75–79.

Aiba, H., Yamada, H., Ohmiya, R., and Mizuno, T. (1995). The osmo-inducible gpd1+ gene is a target of the signaling pathway involving Wis1 MAP-kinase kinase in fission yeast. FEBS Lett. *376*, 199–201.

Akhtar, N., Påhlman, A.K., Larsson, K., Corbett, A.H., and Adler, L. (2000). SGD1 encodes an essential nuclear protein of Saccharomyces cerevisiae that affects expression of the GPD1 gene for glycerol 3-phosphate dehydrogenase. FEBS Lett. *483*, 87–92.

Albertyn, J., Hohmann, S., Thevelein, J.M., and Prior, B.A. (1994). GPD1, which encodes glycerol-3-phosphate dehydrogenase, is essential for growth under osmotic stress in Saccharomyces cerevisiae, and its expression is regulated by the high-osmolarity glycerol response pathway. Mol. Cell. Biol. *14*, 4135–4144.

Aruoma, O.I., Halliwell, B., Hoey, B.M., and Butler, J. (1988). The antioxidant action of taurine, hypotaurine and their metabolic precursors. Biochem. J. *256*, 251–255.

Bao, S., Wu, Q., McLendon, R.E., Hao, Y., Shi, Q., Hjelmeland, A.B., Dewhirst, M.W., Bigner, D.D., and Rich, J.N. (2006). Glioma stem cells promote radioresistance by preferential activation of the DNA damage response. Nature *444*, 756–760.

Basel-Vanagaite, L., Zevit, N., Har Zahav, A., Guo, L., Parathath, S., Pasmanik-Chor, M., McIntyre, A.D., Wang, J., Albin-Kaplanski, A., Hartman, C., et al. (2012). Transient infantile hypertriglyceridemia, fatty liver, and hepatic fibrosis caused by mutated GPD1, encoding glycerol-3-phosphate dehydrogenase 1. Am. J. Hum. Genet. *90*, 49–60.

Bergsland, M., Werme, M., Malewicz, M., Perlmann, T., and Muhr, J. (2006). The establishment of neuronal properties is controlled by Sox4 and Sox11. Genes Dev. *20*, 3475–3486.

Chen, J., Li, Y., Yu, T.S., McKay, R.M., Burns, D.K., Kernie, S.G., and Parada, L.F. (2012). A restricted cell population propagates glioblastoma growth after chemotherapy. Nature *488*, 522–526.

Chino, H. (1957). Conversion of glycogen to sorbitol and glycerol in the diapause egg of the bombyx silkworm. Nature *180*, 2.

Chong, J., Soufan, O., Li, C., Caraus, I., Li, S., Bourque, G., Wishart, D.S., and Xia, J. (2018). MetaboAnalyst 4.0: towards more transparent and integrative metabolomics analysis. Nucleic Acids Res. *46* (W1), W486–W494.

Cimmino, L., Abdel-Wahab, O., Levine, R.L., and Aifantis, I. (2011). TET family proteins and their role in stem cell differentiation and transformation. Cell Stem Cell *9*, 193–204.

Clarke, M.F., Dick, J.E., Dirks, P.B., Eaves, C.J., Jamieson, C.H., Jones, D.L., Visvader, J., Weissman, I.L., and Wahl, G.M. (2006). Cancer stem cells–perspectives on current status and future directions: AACR Workshop on cancer stem cells. Cancer Res. *66*, 9339–9344.

Clevers, H. (2011). The cancer stem cell: premises, promises and challenges. Nat. Med. *17*, 313–319.

Costa, B., Eisemann, T., Strelau, J., Spaan, I., Korshunov, A., Liu, H.K., Bugert, P., Angel, P., and Peterziel, H. (2019). Intratumoral platelet aggregate formation in a murine preclinical glioma model depends on podoplanin expression on tumor cells. Blood Adv. *3*, 1092–1102.

Darmanis, S., Sloan, S.A., Croote, D., Mignardi, M., Chernikova, S., Samghababi, P., Zhang, Y., Neff, N., Kowarsky, M., Caneda, C., et al. (2017). Single-Cell RNA-Seq Analysis of Infiltrating Neoplastic Cells at the Migrating Front of Human Glioblastoma. Cell Rep. *21*, 1399–1410.

Demuth, T., and Berens, M.E. (2004). Molecular mechanisms of glioma cell migration and invasion. J. Neurooncol. *70*, 217–228.

Dobin, A., Davis, C.A., Schlesinger, F., Drenkow, J., Zaleski, C., Jha, S., Batut, P., Chaisson, M., and Gingeras, T.R. (2013). STAR: ultrafast universal RNA-seq aligner. Bioinformatics *29*, 15–21.

Dyer, M.A., Livesey, F.J., Cepko, C.L., and Oliver, G. (2003). Prox1 function controls progenitor cell proliferation and horizontal cell genesis in the mammalian retina. Nat. Genet. *34*, 53–58.

Feng, W., Khan, M.A., Bellvis, P., Zhu, Z., Bernhardt, O., Herold-Mende, C., and Liu, H.K. (2013). The chromatin remodeler CHD7 regulates adult neurogenesis via activation of SoxC transcription factors. Cell Stem Cell *13*, 62–72.

Foster, D.A. (2013). Phosphatidic acid and lipid-sensing by mTOR. Trends Endocrinol. Metab. *24*, 272–278.

Gerke, V., Creutz, C.E., and Moss, S.E. (2005). Annexins: linking Ca2+ signalling to membrane dynamics. Nature Rev. *6*, 449–461.

Gravendeel, L.A., Kouwenhoven, M.C., Gevaert, O., de Rooi, J.J., Stubbs, A.P., Duijm, J.E., Daemen, A., Bleeker, F.E., Bralten, L.B., Kloosterhof, N.K., et al. (2009). Intrinsic gene expression profiles of gliomas are a better predictor of survival than histology. Cancer Res. *69*, 9065–9072.

Hemmati, H.D., Nakano, I., Lazareff, J.A., Masterman-Smith, M., Geschwind, D.H., Bronner-Fraser, M., and Kornblum, H.I. (2003). Cancerous stem cells can arise from pediatric brain tumors. Proc. Natl. Acad. Sci. USA *100*, 15178–15183.

Holland, E.C. (2001). Brain tumor animal models: importance and progress. Curr. Opin. Oncol. *13*, 143–147.

Hu, Y., and Smyth, G.K. (2009). ELDA: extreme limiting dilution analysis for comparing depleted and enriched populations in stem cell and other assays. J. Immunol. Methods *347*, 70–78.

Huang, W., Sherman, B.T., and Lempicki, R.A. (2009). Systematic and integrative analysis of large gene lists using DAVID bioinformatics resources. Nat. Protoc. *4*, 44–57.

Hussy, N., Deleuze, C., Pantaloni, A., Desarménien, M.G., and Moos, F. (1997). Agonist action of taurine on glycine receptors in rat supraoptic magnocellular neurones: possible role in osmoregulation. J. Physiol. *502*, 609–621.

Ingolia, N.T. (2014). Ribosome profiling: new views of translation, from single codons to genome scale. Nat. Rev. Genet. *15*, 205–213.

Ingolia, N.T., Ghaemmaghami, S., Newman, J.R., and Weissman, J.S. (2009). Genome-wide analysis in vivo of translation with nucleotide resolution using ribosome profiling. Science *324*, 218–223.

Ingolia, N.T., Brar, G.A., Rouskin, S., McGeachy, A.M., and Weissman, J.S. (2012). The ribosome profiling strategy for monitoring translation in vivo by deep sequencing of ribosome-protected mRNA fragments. Nat. Protoc. *7*, 1534–1550.

Kaal, E.C., and Vecht, C.J. (2004). The management of brain edema in brain tumors. Curr. Opin. Oncol. *16*, 593–600.

Kim, S., Thiessen, P.A., Bolton, E.E., Chen, J., Fu, G., Gindulyte, A., Han, L., He, J., He, S., Shoemaker, B.A., et al. (2016). PubChem Substance and Compound databases. Nucleic Acids Res. *44* (D1), D1202–D1213.

Koo, B.K., Stange, D.E., Sato, T., Karthaus, W., Farin, H.F., Huch, M., van Es, J.H., and Clevers, H. (2011). Controlled gene expression in primary Lgr5 organoid cultures. Nat. Methods *9*, 81–83.

Krämer, A., Green, J., Pollard, J., Jr., and Tugendreich, S. (2014). Causal analysis approaches in Ingenuity Pathway Analysis. Bioinformatics *30*, 523–530.

Kreso, A., and Dick, J.E. (2014). Evolution of the cancer stem cell model. Cell Stem Cell *14*, 275–291.

Lapidot, T., Sirard, C., Vormoor, J., Murdoch, B., Hoang, T., Caceres-Cortes, J., Minden, M., Paterson, B., Caligiuri, M.A., and Dick, J.E. (1994). A cell initiating human acute myeloid leukaemia after transplantation into SCID mice. Nature *367*, 645–648.

Liao, Y., Smyth, G.K., and Shi, W. (2013). The Subread aligner: fast, accurate and scalable read mapping by seed-and-vote. Nucleic Acids Res. *41*, e108.

Ligon, K.L., Huillard, E., Mehta, S., Kesari, S., Liu, H., Alberta, J.A., Bachoo, R.M., Kane, M., Louis, D.N., Depinho, R.A., et al. (2007). Olig2-regulated lineage-restricted pathway controls replication competence in neural stem cells and malignant glioma. Neuron *53*, 503–517.

Love, M.I., Huber, W., and Anders, S. (2014). Moderated estimation of fold change and dispersion for RNA-seq data with DESeq2. Genome Biol. *15*, 550.

Magee, J.A., Piskounova, E., and Morrison, S.J. (2012). Cancer stem cells: impact, heterogeneity, and uncertainty. Cancer Cell *21*, 283–296.

Metsalu, T., and Vilo, J. (2015). ClustVis: a web tool for visualizing clustering of multivariate data using Principal Component Analysis and heatmap. Nucleic Acids Res. *43* (W1), W566–W570.

Nishino, J., Kim, I., Chada, K., and Morrison, S.J. (2008). Hmga2 promotes neural stem cell self-renewal in young but not old mice by reducing p16Ink4a and p19Arf Expression. Cell *135*, 227–239.

Osswald, M., Jung, E., Sahm, F., Solecki, G., Venkataramani, V., Blaes, J., Weil, S., Horstmann, H., Wiestler, B., Syed, M., et al. (2015). Brain tumour cells interconnect to a functional and resistant network. Nature *528*, 93–98.

Ou, X., Ji, C., Han, X., Zhao, X., Li, X., Mao, Y., Wong, L.L., Bartlam, M., and Rao, Z. (2006). Crystal structures of human glycerol 3-phosphate dehydrogenase 1 (GPD1). J. Mol. Biol. *357*, 858–869.

Park, I.K., Morrison, S.J., and Clarke, M.F. (2004). Bmi1, stem cells, and senescence regulation. J. Clin. Invest. *113*, 175–179.

Patel, A.P., Tirosh, I., Trombetta, J.J., Shalek, A.K., Gillespie, S.M., Wakimoto, H., Cahill, D.P., Nahed, B.V., Curry, W.T., Martuza, R.L., et al. (2014). Single-cell RNA-seq highlights intratumoral heterogeneity in primary glioblastoma. Science *344*, 1396–1401.

Peterziel, H., Müller, J., Danner, A., Barbus, S., Liu, H.-K., Radlwimmer, B., Pietsch, T., Lichter, P., Schütz, G., Hess, J., and Angel, P. (2012). Expression of podoplanin in human astrocytic brain tumors is controlled by the PI3K-AKT-AP-1 signaling pathway and promoter methylation. Neuro-oncol. *14*, 426–439.

Phillips, H.S., Kharbanda, S., Chen, R., Forrest, W.F., Soriano, R.H., Wu, T.D., Misra, A., Nigro, J.M., Colman, H., Soroceanu, L., et al. (2006). Molecular subclasses of high-grade glioma predict prognosis, delineate a pattern of disease progression, and resemble stages in neurogenesis. Cancer Cell *9*, 157–173.

Pietras, A., Katz, A.M., Ekström, E.J., Wee, B., Halliday, J.J., Pitter, K.L., Werbeck, J.L., Amankulor, N.M., Huse, J.T., and Holland, E.C. (2014). Osteopontin-CD44 signaling in the glioma perivascular niche enhances cancer stem cell phenotypes and promotes aggressive tumor growth. Cell Stem Cell *14*, 357–369.

Prochazka, M., Kozak, U.C., and Kozak, L.P. (1989). A glycerol-3-phosphate dehydrogenase null mutant in BALB/cHeA mice. J. Biol. Chem. *264*, 4679–4683.

Pusterla, T., Nèmeth, J., Stein, I., Wiechert, L., Knigin, D., Marhenke, S., Longerich, T., Kumar, V., Arnold, B., Vogel, A., et al. (2013). Receptor for advanced glycation endproducts (RAGE) is a key regulator of oval cell activation and inflammation-associated liver carcinogenesis in mice. Hepatology *58*, 363–373.

Reya, T., Morrison, S.J., Clarke, M.F., and Weissman, I.L. (2001). Stem cells, cancer, and cancer stem cells. Nature *414*, 105–111.

Sanjana, N.E., Shalem, O., and Zhang, F. (2014). Improved vectors and genome-wide libraries for CRISPR screening. Nat. Methods *11*, 783–784.

Singh, S.K., Clarke, I.D., Terasaki, M., Bonn, V.E., Hawkins, C., Squire, J., and Dirks, P.B. (2003). Identification of a cancer stem cell in human brain tumors. Cancer Res. *63*, 5821–5828.

Singh, S.K., Hawkins, C., Clarke, I.D., Squire, J.A., Bayani, J., Hide, T., Henkelman, R.M., Cusimano, M.D., and Dirks, P.B. (2004). Identification of human brain tumour initiating cells. Nature *432*, 396–401.

Sosa, M.S., Bragado, P., and Aguirre-Ghiso, J.A. (2014). Mechanisms of disseminated cancer cell dormancy: an awakening field. Nat. Rev. Cancer *14*, 611–622.

Stupp, R., Taillibert, S., Kanner, A., Read, W., Steinberg, D., Lhermitte, B., Toms, S., Idbaih, A., Ahluwalia, M.S., Fink, K., et al. (2017). Effect of Tumor-Treating Fields Plus Maintenance Temozolomide vs Maintenance Temozolomide Alone on Survival in Patients With Glioblastoma: A Randomized Clinical Trial. JAMA *318*, 2306–2316.

Subramanian, A., Tamayo, P., Mootha, V.K., Mukherjee, S., Ebert, B.L., Gillette, M.A., Paulovich, A., Pomeroy, S.L., Golub, T.R., Lander, E.S., and Mesirov, J.P. (2005). Gene set enrichment analysis: a knowledge-based approach for interpreting genome-wide expression profiles. Proc. Natl. Acad. Sci. USA *102*, 15545–15550.

Suvà, M.L., Rheinbay, E., Gillespie, S.M., Patel, A.P., Wakimoto, H., Rabkin, S.D., Riggi, N., Chi, A.S., Cahill, D.P., Nahed, B.V., et al. (2014). Reconstructing and reprogramming the tumor-propagating potential of glioblastoma stem-like cells. Cell *157*, 580–594.

Team, R.C. (2018). R: A Language and Environment for Statistical Computing (R Foundation for Statistical Computing).

Tirosh, I., Venteicher, A.S., Hebert, C., Escalante, L.E., Patel, A.P., Yizhak, K., Fisher, J.M., Rodman, C., Mount, C., Filbin, M.G., et al. (2016). Single-cell RNA-seq supports a developmental hierarchy in human oligodendroglioma. Nature *539*, 309–313.

Tönjes, M., Barbus, S., Park, Y.J., Wang, W., Schlotter, M., Lindroth, A.M., Pleier, S.V., Bai, A.H.C., Karra, D., Piro, R.M., et al. (2013). BCAT1 promotes cell proliferation through amino acid catabolism in gliomas carrying wild-type IDH1. Nat. Med. *19*, 901–908.

Trapnell, C., Pachter, L., and Salzberg, S.L. (2009). TopHat: discovering splice junctions with RNA-Seq. Bioinformatics *25*, 1105–1111.

Trapnell, C., Roberts, A., Goff, L., Pertea, G., Kim, D., Kelley, D.R., Pimentel, H., Salzberg, S.L., Rinn, J.L., and Pachter, L. (2012). Differential gene and transcript expression analysis of RNA-seq experiments with TopHat and Cufflinks. Nat. Protoc. *7*, 562–578.

Tschaharganeh, D.F., Xue, W., Calvisi, D.F., Evert, M., Michurina, T.V., Dow, L.E., Banito, A., Katz, S.F., Kastenhuber, E.R., Weissmueller, S., et al. (2014). p53-dependent Nestin regulation links tumor suppression to cellular plasticity in liver cancer. Cell *158*, 579–592.

Tunici, P., Bissola, L., Lualdi, E., Pollo, B., Cajola, L., Broggi, G., Sozzi, G., and Finocchiaro, G. (2004). Genetic alterations and in vivo tumorigenicity of neurospheres derived from an adult glioblastoma. Mol. Cancer *3*, 25.

Venteicher, A.S., Tirosh, I., Hebert, C., Yizhak, K., Neftel, C., Filbin, M.G., Hovestadt, V., Escalante, L.E., Shaw, M.L., Rodman, C., et al. (2017). Decoupling genetics, lineages, and microenvironment in IDH-mutant gliomas by single-cell RNA-seq. Science *355*. Published online March 31, 2017. https://doi.org/10.1126/science.aai8478.

Verhaak, R.G., Hoadley, K.A., Purdom, E., Wang, V., Qi, Y., Wilkerson, M.D., Miller, C.R., Ding, L., Golub, T., Mesirov, J.P., et al.; Cancer Genome Atlas Research Network (2010). Integrated genomic analysis identifies clinically relevant subtypes of glioblastoma characterized by abnormalities in PDGFRA, IDH1, EGFR, and NF1. Cancer Cell *17*, 98–110.

Vescovi, A.L., Galli, R., and Reynolds, B.A. (2006). Brain tumour stem cells. Nat. Rev. Cancer *6*, 425–436.

Wang, Y., Liu, H.-K., and Schütz, G. (2013). Role of the nuclear receptor Tailless in adult neural stem cells. Mech. Dev. *130*, 388–390.

Wen, P.Y., and Kesari, S. (2008). Malignant gliomas in adults. N. Engl. J. Med. *359*, 492–507.

Wishart, D.S., Feunang, Y.D., Marcu, A., Guo, A.C., Liang, K., Vázquez-Fresno, R., Sajed, T., Johnson, D., Li, C., Karu, N., et al. (2018). HMDB 4.0: the human metabolome database for 2018. Nucleic Acids Res. *46* (D1), D608–D617.

Zhang, C.L., Zou, Y., He, W., Gage, F.H., and Evans, R.M. (2008). A role for adult TLX-positive neural stem cells in learning and behaviour. Nature *451*, 1004–1007.

Zhong, X., Liu, X., Li, Y., Cheng, M., Wang, W., Tian, K., Mu, L., Zeng, T., Liu, Y., Jiang, X., et al. (2016). HMGA2 sustains self-renewal and invasiveness of glioma-initiating cells. Oncotarget *7*, 44365–44380.

Zhu, Z., Khan, M.A., Weiler, M., Blaes, J., Jestaedt, L., Geibert, M., Zou, P., Gronych, J., Bernhardt, O., Korshunov, A., et al. (2014). Targeting self-renewal in high-grade brain tumors leads to loss of brain tumor stem cells and prolonged survival. Cell Stem Cell *15*, 185–198.

STAR★METHODS

KEY RESOURCES TABLE

REAGENT or RESOURCE	SOURCE	IDENTIFIER
Antibodies		
Rabbit polyclonal anti-GPD1	Abcam	Cat#ab153902
Mouse monoclonal anti-PCNA (PC10)	Millipore	Cat#NA03; RRID:AB_2160355
Rabbit polyclonal anti-Ki67	Abcam	Car#ab15580; RRID:AB_443209
Chicken polyclonal anti-GFP	Abcam	Cat# ab13970, RRID:AB_300798
Rat monoclonal anti-BrdU	Abcam	Cat# ab6326, RRID:AB_305426
Goat polyclonal anti-OLIG2	Santa Cruz	Cat# sc-19969, RRID:AB_2236477
Mouse monoclonal anti-SOX2	ThermoFisher Scientific	Cat# MA1-014, RRID:AB_2536667
Mouse monoclonal anti-Nestin	BD Biosciences	Cat# 556309, RRID:AB_396354
Rat monoclonal anti-CD34	Abcam	Cat# ab8158, RRID:AB_306316
Mouse monoclonal anti-NeuN (clone A60)	Millipore	Cat# MAB377, RRID:AB_2298772
Rabbit polyclonal anti-RFP	Rockland	Cat# 600-401-379, RRID:AB_2209751
Goat polyclonal anti-m-Cherry (RFP)	SICGEN	Cat# AB0040-500, RRID:AB_2333093
Mouse monoclonal anti-CNPase	Millipore	Cat# MAB326, RRID:AB_2082608
Rabbit monoclonal anti-S6 ribosomal protein	Cell Signaling Technology	Cat# 2217, RRID:AB_331355
Rabbit mooclonal anti-phospho-S6 ribosomal protein	Cell Signaling Technology	Cat# 4858, RRID:AB_916156
Rabbit monoclonal anti-AKT (pan)	Cell Signaling Technology	Cat# 4685, RRID:AB_2225340
Rabbit polyclonal anti-phospho-AKT	Cell Signaling Technology	Cat# 9271, RRID:AB_329825
Rabbit monoclonal anti-p44/42 MAPK (Erk1/2)	Cell Signaling Technology	Cat# 4695, RRID:AB_390779
Rabbit monoclonal anti-phospho-p44/42 MAPK (Erk1/2) (Thr202/Tyr204) (20G11)	Cell Signaling Technology	Cat# 4376, RRID:AB_331772
Rabbit polyclonal anti-ANXA6	Sigma-Aldrich	Cat#HPA009650, RRID:AB_1844867
Mouse monoclonal anti-FLAG M2	Sigma-Aldrich	Cat# F1804, RRID:AB_262044
Mouse monoclonal anti-Ki67	BD Biosciences	Cat# 550609, RRID:AB_393778
Chemicals, Peptides, and Recombinant Proteins		
Temozolomide	Sigma-Aldrich	T2577
Tamoxifen	Sigma-Aldrich	T5648-5G
DMSO molecular biology grade	Sigma-Aldrich	D8418-50ML
Luciferin	Biocat	7903-100-BV
DMEM/F-12	Life technologies	31330095
B27 supplement	Life technologies	12587010
Laminin	Roche Diagnostics	11243217001
Trypsin 2.5%	Life Technologies	15090046
EGF	Sigma-Aldrich	F0291-25UG
FGF	Sigma-Aldrich	F0291-25UG
DMEM Glutamax	Life Technologies	31966047
Accutase	Sigma-Aldrich	A6964-100ML
PLL	Sigma-Aldrich	P2636-100MG
Deposited Data		
Sequencing results	GEO repository	GEO: GSE110869
Sequencing results	GEO repository	GEO: GSE110866
Sequencing results	GEO repository	GEO: GSE110867
Sequencing results	GEO repository	GEO: GSE110868

(*Continued on next page*)

Continued

REAGENT or RESOURCE	SOURCE	IDENTIFIER
Experimental Models: Cell Lines		
Primary mouse NSCs	This study	NA
Primary mouse BTSCs	This study	NA
Human glioma stem cells	University Hospital, Heidelberg Universtiy	NA
DF1 cells	ATCC	VR-1828
HEK293T	ATCC	CRL-1573
Experimental Models: Organisms/Strains		
Ntv-a mouse	JAX Lab	Tg(NES-TVA)J12Ech
Ntv-a/Tlx-GFP mouse	Zhu et al., 2014	NA
Ntv-a/Nes-CreERT2 mouse	Zhu et al., 2014	NA
PTEN;p53/Tlx-CreERT2 mouse	Peterziel et al., 2012	NA
Oligonucleotides		
GPD1miRNA:AAAGTTGGGTGTCTGCATCAGGTTT TGGCCACTGACTGACCTGATGCACACCCAACTTT	Sigma-Aldrich	N/A
Control-miRNA: AAATGTACTGCGCGTGGAGACGT TTGGCCACTGACTGACGTCTCCACGCAGTACATTT	Sigma-Aldrich	NA
GPD1 guide RNA1: AAAGTCTGCATTGTCGGCTC	Sigma-Aldrich	NA
GPD1 guide RNA2: TGCATTGCTACCCACGATCT	Sigma-Aldrich	NA
GPD1 shRNA3: CCGGGCCACCACATTTGCCAGAAA TCTCGAGATTTCTGGCAAATGTGGTGGCTTTTTG	Sigma-Aldrich	NA
GPD1 shRNA5: CCGGCCATCAGTTCATCGGCAAGAT CTCGAGATCTTGCCGATGAACTGATGGTTTTTG	Sigma-Aldrich	NA
GPD1 shRNA7: CCGGGCGTACAGGAAAGTCCATTG ACTCGAGTCAATGGACTTTCCTGTACGCTTTTTG	Sigma-Aldrich	NA
GPD1 shRNA9: CCGGGCAGACACCAAACTTCCGTA TCTCGAGATACGGAAGTTTGGTGTCTGCTTTTT	Sigma-Aldrich	NA
shNT: SHC002 from Sigma	Sigma-Aldrich	NA
Software and Algorithms		
ImageJ		https://imagej.net/Welcome
RNAi designer		https://rnaidesigner.thermofisher.com/rnaiexpress/
CRISPR design tool@		http://zlab.bio/guide-design-resources
STAR		https://github.com/alexdobin/STAR
R		https://www.r-project.org/
DAVID		https://david.ncifcrf.gov/
DESeq2		https://bioconductor.org/packages/release/bioc/html/DESeq2.html
MetaboAnalyst		https://www.metaboanalyst.ca/
Ingenuity Pathway Analysis		https://www.qiagenbioinformatics.com/products/ingenuity-pathway-analysis/
WGCNA		https://horvath.genetics.ucla.edu/html/CoexpressionNetwork/Rpackages/WGCNA/
Human Metabolome Databasse		http://www.hmdb.ca/
Lipid maps		https://www.lipidmaps.org/
Pubchem database		https://pubchem.ncbi.nlm.nih.gov/search/
GSEA		https://software.broadinstitute.org/gsea/index.jsp
bowtie2		http://bowtie-bio.sourceforge.net/bowtie2/index.shtml

(*Continued on next page*)

Continued

REAGENT or RESOURCE	SOURCE	IDENTIFIER
tophat		https://ccb.jhu.edu/software/tophat/index.shtml
cuffdiff		https://cole-trapnell-lab.github.io/cufflinks/cuffdiff/
Xcalibur		https://www.thermofisher.com/order/catalog/product/OPTON-30487
Progenesis QI		http://www.nonlinear.com/progenesis/qi/
clustvis		https://biit.cs.ut.ee/clustvis/

LEAD CONTACT AND MATERIALS AVAILABILITY

Further information and requests for resources and reagents should be directed to and will be fulfilled by the Lead Contact, Hai-Kun Liu (l.haikun@dkfz.de)

EXPERIMENTAL MODEL AND SUBJECT DETAILS

Mouse lines

The Ntv-a mouse was kindly provided by Eric Holland and is available from Jackson Laboratories. The Tlx-GFP reporter animal was obtained from the GENSAT project. The Nes-TVA/Nestin-CreERT2 mouse line was generated by crossing these two lines, which are both available from Jackson Laboratories, and has been successfully used to target brain tumor cells via tamoxifen injection (Zhu et al., 2014). All animal experiments were conducted according to animal welfare regulations and have been approved by the responsible authorities (Regierungspräsidium Karlsruhe). PTEN;p53;Tlx-CreERT2 mice were generated by crossing Tlx-CreERT2 and PTEN ^{flox};p53^{flox} mice(Peterziel et al., 2012). Tamoxifen was used to induce recombination in 7-8 weeks old mice and mouse tumor stem cells were isolated for cell culture. Brain tumors were induced in newborn Nes-TVA mice and they were sacrificed when they showed symptoms. For each experiment, several breedings were set up and all the siblings were used as the Cre- mice served as control for the Cre+ mice. We use both male and females in this study and not sex-associated phenotype were observed. The animals were not involved in any previous procedures.

Mouse housing

All animals were housed in "open" type 1L (1145T) cages (Tecniplast Deutschland GmbH, Bahnhofstr. 69, D-82383 Hohenpeißenberg) at the Center for Preclinical Research of the DKFZ under strict specified pathogen-free (SPF) conditions according to the recommendations of the FELASA. The light / dark cycle was adjusted to 12 h lights-on and 12 h lights-off with the beginning of the light and dark period set at 7.00 and 19.00, respectively. Autoclaved decalcified water and food pellets (Kliba Nafag, Rinaustrasse 380, CH-4303 Kaiseraugst) were given *ad libitum*. In accordance with the Appendix A of the European Convention for the Protection of Vertebrate Animals used for Experimental and Other Scientific Purposes from 18th March 1986 room temperature and relative humidity were adjusted to 22.0 ± 2.0°C and 55.0 ± 10.0%, respectively. For routine health monitoring, colony animals, contact and soiled bedding sentinels (in dependence on the housing conditions and the unit's purpose) were periodically tested for viral and bacterial infections, and parasites. Breeding units and larger experimental units were monitored every week with at least 2-4 animals tested. Additionally, diagnostics of sick animals was performed whenever necessary. The health monitoring program fulfils and exceeds the criteria – in terms of number of animals, frequency of monitoring, age, agents and methods – as given in the FELASA recommendations for the health monitoring of mouse colonies in Breeding and Experimental Units. The SPF experimental units at the DKFZ are free of all FELASA listed agents (pathogens and opportunists) plus Corynebacterium bovis except for the following agents which are regularly found: murine norovirus, apathogenic flagellates, *Helicobacter* spp., Rodentibacter spp. and Muribacter muris (members of the Pasteurellaceae family), and less often Pneumocystis murina and Staphylococcus aureus.

Tumor induction

The RCAS-PDGFB/AKT vectors were used for induction of the brain tumors in Ntv-a, Ntv-a/ Nestin-CreERT2, Ntv-a/Tlx-GFP mice (Zhu et al., 2014). Additionally, the following vectors were used as well: RCAS-GFP to mark the tumor cells with GFP, RCAS-Luciferase to monitor tumor growth, RCAS-*Gpd1*-microRNA and RCAS-control-microRNA. DF-1 cells, an immortalized chicken cell line purchased from ATCC, were individually transfected with Fugene (Promega) and the desired vector. After two days, the DF-1 cells were collected and 20,000 cells were injected for each vector into the left SVZ of newborn mice. The injection volume was 1 μl. For survival studies, mice were closely monitored by blinded animal caretakers and sacrificed when neurological symptoms occurred.

Human samples

For IF analysis of human GBM samples, GBM specimens (n = 5) were obtained from patients undergoing surgical resection at the Department of Neurosurgery at the University Hospital Heidelberg, Germany. Use of patient material was approved by the Institutional Review Board at the Medical Faculty Heidelberg. Informed consent was obtained from all patients included in the study.

Cultivation of human glioma stem cells

Cells were cultured in DMEM-Ham F-12 (Biochrom), 1% PenStrep (Life Technologies), 2 mM L-GLutamax (GIBCO), 20% BIT supplement (Stem Cell Technology), 20ng/ml Epidermal growth factor (human, recombinant, Promocell) and 20ng/ml Fibroblast growth factor 2 (human, Promocell). Cells were split approx. every 3 days.

Treatments of mice

Tamoxifen (Sigma) was dissolved in sunflower seed oil (Sigma) with 10% $EtOH_{abs}$ to prepare a 10 mg ml^{-1} solution. Intraperitoneal injections were performed with 1 mg/day for 10 days. BrdU was dissolved in sterile 0.9% saline to prepare a 15 mg ml^{-1} solution, and mice were injected intraperitoneally with 300 mg kg^{-1} 2 hr before sacrifice for short-term BrdU tracing or for 5 consecutive days, once daily, for long-term tracing. TMZ (Sigma) was dissolved in DMSO and freshly diluted in 0.9% saline (5 mg/ml) and injected intraperitoneally with 100 mg kg^{-1}/day for 5 days.

The tumor growth of TMZ or DMSO treated mice was monitored by Bioluminescence Imaging (BLI) using the IVIS Lumina II *In Vivo* Imaging System (Perkin Elmer). The expressed luciferase in the mouse brain tumors converts the substrate D-luciferin intooxyluciferin and produces light. Animals were given an injection of D-luciferin (Biocat, 7903-1g-BV) intraperitoneally at a concentration of 150 mg/kg of body weight. Following the injection, animals were anesthetized using the XGI-8 system provided with the IVIS and imaged by taking one picture every minute. The used parameters were: exposure time: 1 min (in the case of the signal being too high, the exposure time was reduced to 30 s, 15 s or 5 s to avoid overexposure), high binning and aperture lens position: F1. The light was detected by the IVIS system and displayed as a pixel image, overlapping with a photograph of the animals being imaged. A Region of Interest (ROI) was then drawn over the head of the mouse using the Living Image 4.3.1 software provided with the IVIS system and the total signal was calculated in photon/sec (p/s). Measurements were taken until the signal decreased again and the highest signal for each mouse was taken

Mouse cell lines

Mouse SVZs (pooled from 3 animals) and brain tumors were dissected in 5 mL solution 1 (0.05% trypsin-EDTA, 1x HBSS, 2 mM D-glucose, 15 mM HEPES), incubated at 37°C for 30 min and repeatedly triturated. The cell suspension was mixed with an equal volume of ice-cold solution 2 (4% w/v BSA, 20 mM HEPES, 1x EBSS), passed through a 70 μm strainer and centrifuged at 1200 rpm for 5 min. The supernatant was removed and the cells were resuspended in ice-cold solution 3 (0.5x HBSS, 1 M sucrose) and centrifuged at 2000 rpm for 20 min. The cell pellet was resuspended in 2 mL solution2 and placed on top of 12 mL solution2 in a new tube. After centrifugation at 1500 rpm for 9 min the cell pellet was resuspended in culture medium and the cells were grown as neurospheres. To establish monolayer culture, neurospheres were dissociated with Accutase (Sigma-Aldrich) and were seeded on laminin (Roche) and poly-L-lysine (Sigma-Aldrich)-coated cell culture plates.

Dissociated cells were kept in DMEM/F12 medium containing 20 ng ml^{-1} EGF (Sigma-Aldrich), 10 ng ml^{-1} FGF2 (Sigma-Aldrich), B27 (GIBCO), and ITSS (Roche). The medium was renewed every 3 days. As we mostly use low passage primary cells in our study, authentication is not necessary.

DF-1 cells, which were used for virus production to induce brain tumors, are an immortalized chicken cell line and were purchased from ATCC (VR-1828), which were authenticated.

METHOD DETAILS

Ribosome Profiling and mRNA sequencing

The ribosome profiling experiment with primary NSCs and BTSCs was performed as described previously with minor changes (Ingolia et al., 2012). The cells of a 15 cm culture plate were lysed with lysis buffer (20 mM Tris-HCl pH 7.4, 10 mM MgCl2, 200 mM KCl, 1% Triton, 2 mM DTT, 100 μg/ml Cyclohexamide, 25 U/ml DNase and EDTA-free protease inhibitors, Roche). The mRNA not protected by ribosomes was digested with RNaseI and ribosomes were collected by centrifugation with a continuous sucrose gradient (10%–50%) with DTT, cyclohexamideand 20 U/ml SUPERaseIN. RNA was isolated by acid phenol extraction and precipitated. Precipitated RNA was resuspended in 10 mM Tris pH7, mixed with 2x sample buffer (TBE-urea, NOVEX, Invitrogen) and loaded on a 15% TBE-urea gel. The gel fragment containing RNA fragments between 26-34 nt was excised and used for library generation exactly as described previously (Ingolia et al., 2012). The library was sequenced on the Illumina HiSeq system according to the manufacturer's protocol.

For RNA isolation from cultured NSCs, BTSCs and GPD1-KO BTSCSs cells were harvested in TRI Reagent (Sigma) following the protocol. After chloroform phase separation, the transparent upper phase was added to an equal volume of 70% ethanol and transferred to an RNeasy Mini spin column (QIAGEN). The RNA was purified according to the protocol and send for library preparation and Illumina HiSeq sequencing to our in-house facility.

Cell culturing for metabol/lipid-omics experiments

All cell lines were cultured for 3 days as a monolayer culture in 10 cm dishes until they reached a concentration of approximately $3x10^6$ cells per ml. When reached to the desired confluency, cells were washed twice with cold PBS. After washing, 5 mL of ice-cold methanol was added to the monolayer, cells were harvested from the plate into a 15 mL Falcon tubes. Methanol extracts were then sonicated for 10 min ice and vortexed for 5 min. The methanol extracts were then removed by centrifugation and dried under a stream of nitrogen gas. The dried samples were resuspended in mobile phase and 20 μL of each was injected into the LC-MS system.

LC-MS/MS experiments for metabolomics

LC-MS/MS analysis was performed on a Vanquish UHPLC system coupled to a Q-Exactive plus HRMS (Thermo Scientific, MA, USA) in both ESI positive and negative mode. The separation of metabolites was carried out on Waters Xbridge Amide (100X 2.1mm; 2.6uM) at the flow rate of 0.3 ml/min and maintained at 40°C. The mobile phase consisted of solvent A (7.5 mM Ammonium acetate with 0.05% NH4OH) and solvent B (acetonitrile). Metabolites were detected with HRMS full scan at the mass resolving power R = 70000 in mass range of 60-900 m/z. The data-dependent tandem (MS/MS) mass scans were obtained along with full scans using higher energy collisional dissociation (HCD) of normalized collision energies of 10, 20 and 40 units which were at the mass resolving power R = 17500. The MS parameters in the Tune software (Thermo Scientific) were set as; spray voltage of 4 kV (for negative mode 3.5 kV), sheath gas 30 and auxiliary gas 5 units, S-Lens 65 eV, capillary temperature 320°C and vaporization temperature of auxiliary gas was 300°C. Data was acquired in full scan mode and data dependent tandem mass spectra (MS/MS) for the top 10 most intense precursors ions.

All samples were randomized during LC-MS analysis sequence. The pooled quality control (QC) samples were prepared by mixing equal volume from each sample and processed in a similar manner. Blank and multiple QC samples were injected at the beginning of the sample analysis sequence in order to stabilize the LC-MS system. A QC sample was injected after every 4 samples to track the stability of the instrument and of the analytical method (%CV < 20) throughout the analysis sequence. The chromatograms were evaluated manually and stability of QC samples was checked with principal component analysis (PCA) plots before proceeding for further data analysis.

The Thermo Xcalibur software (Thermo Scientific, MA, USA) was used for data acquisition and preliminary data analysis, including evaluation of chromatogram quality and obtaining extracted ion chromatograms (XIC), peak integration and raw data visualization. LC-MS/MS data alignment, peak picking, adduct deconvolution, normalization, and identification was performed using Progenesis QI (Waters, Nonlinear Dynamics, UK) software. Metabolite annotations were performed using HMDB database and EMBL Metabolomics Core Facility spectral library (http://curatr.mcf.embl.de) for MS and MS/MS-based identification. The mass tolerance in MS1 and MS2 was 5 ppm and 10 ppm, respectively.

LC-MS/MS experiments for lipidomics

The Lipids extraction followed the instructions in https://www.embl.de/mcf/metabolomics-core-facility/protocols/index.html. LC-MS/MS analysis was performed on a Vanquish UHPLC system coupled to a Q-Exactive plus HRMS (Thermo Scientific, MA, USA) in both ESI positive and negative mode. The separation of lipids and fatty acids was carried out on Agilent Poroshell (3 × 50mm; 2.7 μM) at a flow rate of 0.26 ml/min and maintained at 40°C. The mobile phase consisted of solvent A (acetonitrile-water (6:4)) and solvent B (isopropyl alcohol−acetonitrile (9:1)), which were buffered with 10 mM ammonium acetate for negative mode analysis and with 10 mM ammonium formate for positive mode analysis.

Lipids were detected with HRMS full scan at the mass resolving power R = 70000 in a mass range of 200-1500 m/z. The data-dependent tandem (MS/MS) mass scans were obtained along with full scans using higher energy collisional dissociation (HCD) with normalized collision energies of 20, 30 and 40 units which were at the mass resolving power R = 17500. The MS parameters in the Tune software (Thermo Scientific) were set as spray voltage of 4 kV, sheath gas 30 and auxiliary gas 5 units, S-Lens 65 eV, capillary temperature 320°C and vaporization temperature of auxiliary gas was 300°C. Data was acquired in full scan mode and data dependent tandem mass spectra (MS/MS) were obtained for the top 10 most intense precursors.

All samples were randomized for LC-MS analysis sequence. The pooled quality control (QC) samples were prepared by mixing equal volume from each sample and were processed in a similar manner as the samples. Blank and multiple QC samples were injected at the beginning of the sample analysis sequence in order to stabilize the LC-MS system. A QC sample was injected after every 6 samples to track the stability of the instrument and of the analytical method (%CV < 20) throughout the analysis sequence. The chromatograms were evaluated manually and stability of QC samples was checked with principal component analysis (PCA) plots before proceeding for further data analysis.

The Thermo Xcalibur software (Thermo Scientific, MA, USA) was used for data acquisition and preliminary data analysis, including evaluation of chromatogram quality and obtaining extracted ion chromatograms (XIC), peak integration and raw data visualization. LC-MS/MS data alignment, peak picking, adduct deconvolution, normalization, and identification was performed using Progenesis QI (Waters, Nonlinear Dynamics, UK) software. Lipid annotations were performed using LipidBlast database and EMBL Metabolomics Core Facility spectral library (http://curatr.mcf.embl.de) for MS and MS/MS-based identification. The mass tolerance in MS1 and MS2 was 5 ppm and 10 ppm respectively.

Immunohistochemistry and Western Blots

Mice were perfused with 4% paraformaldehyde, and the brains were post fixed overnight at 4°C. Vibratome sections (50 μm) or 5 μm paraffin sections were blocked in 5% normal swine serum in PBST (PBS + 0.2% Triton X-100) and incubated overnight at 4°C with the primary antibody. Fluorescent images were captured using a confocal laser-scanning microscope (LSM800, Zeiss) or a motorized widefield slide scanner (Axios Scan Z1, Zeiss). For imaging stitching, the images were acquired under the Tile Scan mode of Zeiss LSM800 and images were automatically stitched together. Primary antibodies used above are: GPD1 (1:200, abcam, ab153902), PCNA (1:200, Calbiochem, NA03), Ki67 (1:500, abcam, ab15580), GFP (1:500, abcam, 13970), BrdU (1:500, abcam, ab6323), OLIG2 (1:100, Santa Cruz, sc-19969), SOX2 (1:200, Invitrogen, MA1-014), NESTIN(1:200, BD Pharmigen, 556309), CD34 (1:200, abcam, ab8158), NeuN (1:200, Millipore, MAB377), RFP (1:500, Rockland, 600-401-379), m-Cherry (1:500, Acris, AB0040), CNPase (1:200, Millipore, MAB326), p-S6 (1:200, Cell Signaling, 4858). The species-specific Alexa Fluor labeled secondary antibodies were obtained from Invitrogen and used as a 1:400 dilution.

Cryosections (5-7 μm) were prepared from snap-frozen tumor tissues. All slides were dried overnight, acetone-fixed (10 min., −20°C) and stained with an optimized concentration of primary antibodies (mouse anti-Ki-67 (#550609, BD Biosciences); rabbit anti-GPD1 (#ab153902; Abcam)) and the appropriate isotype controls (IgG: #ab27478, and IgG1: #ab91353, both Abcam) for 1h followed by three washing steps with 1x DPBS (#14190094, Invitrogen) including 0.05% Tween20 (#A151.1, Carl Roth). Detection was performed by using fluorochrome-conjugated secondary antibodies (anti-mouse AF647 (#A-21463, Invitrogen), anti-rabbit AF488 (#A-21441, Invitrogen), DAPI (1:1000; #D1306, ThermoFisher) in DPBS for 1h followed by three washing steps. Finally, slides were mounted with Elvanol (Roth, Karlsruhe, Germany). An Olympus IX51 microscope equipped with an F-View II camera was used for the detection of fluorescent signals (both Olympus, Hamburg, Germany).

For western blot, protein extracts cultured brain tumor stem cells were subjected to electrophoresis and transferred onto a PVDF membrane for immunoblot analysis. The blots were incubated over night with the following primary antibodies: beta tubulin (1:1000, Cell Signaling, 2128), GPD1 (1:200, abcam, ab153902), ANXA6 (1:200, Sigma, HPA009650), FLAG (1:1000, Sigma, F1804), GFP (1:500, abcam, ab13970), AKT (1:1000, Cell Signaling, 4685), p-AKT (1:200, Cell Signaling, 9271), ERK (1:1000, Cell Signaling, 4695), p-ERK (1:200, Cell Signaling, 4376), S6 (1:5000, Cell Signaling, 2217), p-S6 (1:500, Cell Signaling, 4858). The species specific HRP conjugated secondary antibodies were ordered from Santa Cruz and used as a 1:5000 dilution

Cell Culture Experiments

For the differentiation of NSCs and BTSCs, the cells were dissociated with Accutase, and 5×10^4 cells were seeded on laminin and poly-L-lysine-coated coverslips in one well of a 24-well plate. Cells were cultured for 7 days in NSC medium without EGF and with 5 ng ml^{-1} FGF2 and for 7 days in NSC medium without EGF or FGF. After 14 days, the coverslips were collected for analysis. They were washed twice with PBS and incubated for at least 30 min with 4% PFA. After another wash, the cells were incubated for 20 min in PBS with 0.5% Triton and for 1 h in 5% NSS. The primary antibody was left over night at 4°C. After 3 washes the secondary antibody was incubated for 2 h at room temperature. The coverslips were washed, mounted with DAPI containing mounting medium and analyzed with a confocal laser-scanning microscope (LSM800, Zeiss).

For the limiting dilution assay of Pten;Trp53 KO BTSCs, 1, 2, 5, 10, 15 and 20 cells were seeded into 48 wells of a 96 well plate each. The human BTSCs were seeded as 5, 10, 15 and 20 cells per well. After 2 weeks, the number of wells which had neurospheres were counted.

Lentiviral production and GPD1 shRNA knockdown in human glioma stem cells

Lentiviral production was carried out as reported earlier (Tönjes et al., 2013). Glioma Stem Cells (NCH601 and NCH663) were infected during seeding in the presence of 0.8μg/ml polybrene (Millipore) to achieve transduction efficiencies larger than 85%. Lentiviruses contained one non-targeting control shRNA (SHC002) and four shRNAs targeting different regions in GPD1 (TRCN0000026517, TRCN0000026521, TRCN0000157054 and TRCN0000026507, Mission Sigma-Aldrich). Medium replacement was conducted 24 h post infection. Efficiency of infection was determined based on the amount of GFP-positive cells (pLKO.1puro TurboGFPTM) at day 5 in a FACS Canto IITM flow cytometer (BD Biosciences). RNA and protein were collected after 5 days of lenti-virus transduction. RT-PCR and western blotting were carried out to determine the GPD1 knockdown efficiency.

Cloning and validation if GPD1 KD microRNA construct

Invitrogen's RNAi Designer was used to design four different GPD1 miRNAs. These constructs were cloned into a modified pcDNA3.1(+) vector, which had a GFP gene and BsmBI sides for inserting the miRNAs. This vector was co-transfected with FLAG-tagged GPD1 in another pcDNA3.1(+) into HEK293T cells to test the efficiency of the miRNAs. The most efficient miRNA was cloned with BsmBI into a helping vector containing the construct described in Figure 4b and from that vector with ClaI into the RCAS vector, which was used to transfect DF1 cells for virus production. The miRNA used for GPD1 KD had the following sequence AAAGTTGGGTGTCTGCATCAGGTTTTGGCCACTGACTGACCTGATGCACACCCAACTTT containing of a 21 bp antisense targeting sequence, a loop and nucleotides 1-8 and 11-21 of the sense target sequence. While the Invitrogen Designer toll does check for off target effects and only suggests microRNAs with seven or more mismatches, the chosen microRNA sequence was also blasted. The results can be found in Table S4. Except of three genes (*BC016548* long non-coding RNA, *Umad1* and Sap25)

all hits with seven or eight mismatches were only predicted genes. Analysis of RNA sequencing data of the here used BTSCs showed that these gene have no or very low amounts of reads, making it very unlikely that this microRNA has any off-target effects. The control miRNA had the following sequence AAATGTACTGCGCGTGGAGACGTTTGGCCACTGACTGACGTCTCCACGCAGTA CATTT and is predicted to not target any known vertebrate gene.

Cultivation of pten/p53 knockout cell lines

Cells were cultured in DMEM/F12 Medium (Life Technologies) containing 1X N2 Supplement (100X, Life Technologies, 17502048), 1X Glutamax (100X, Life Technologies)) 20ng/ml Epidermal growth factor (human, recombinant, Promocell), 20ng/ml Fibroblast growth factor 2 (human, Promocell) and 1X PenStrep (100X, Life Technologies). Medium was changed every 2nd day and culture was split at a ratio of 1:2 to 1:4 when spheres started appearing dark in the center using 0.025% Trypsine (0,25%, Life Technologies, 1:10 diluted in full medium) and Trypsine neutralization solution (Promocell, 1:1 diluted in DPBS).

Transfection of pten/p53 knockout cells

Cell transfection was performed using FUGENE Transfection reagent (Promega) following the manufacturer's instructions. 10^5 Cells were seeded into one well of a 24-well-plate and transfected at a DNA/FuGENE ratio of 1:4. 3 days after transfection cells were treated with selection marker (Geneticin, GIBCO).

CRISPR /Cas9 mediated GPD1 KO in cultured BTSCs

For the GPD1 KO with CRISPR /Cas9 the vector lentiCRISPv2 was used following the protocol published by the Zhang lab on the GeCKO (genome-scale CRISPR knock-out) (Sanjana et al., 2014). We used the CRISPR Design tool provided in GeCKO, which is based on the specificity analysis performed in Hsu et al., Nature Biotechnology, 2013. Five gRNAS were used to transfect mouse BTSCs with lipofectamine LTX&PLUS reagent (Invitrogen) according to the manufacturer's protocol. After two days puromycin was added to the media for one week to select transfected cells. These cells were seeded as 1000/10 cm coated dish to grow colonies deriving from one single cell. Once the colonies were visible they were gently picked with a pipette tip and resuspended in a coated 24 well plate to expand. Western blots were performed to confirm the GPD1 KO in the expanded colonies. From the colonies of interest DNA was purified and sequenced to prove the GPD1 KO. All five gRNAs could knock-out GPD1. We chose the two gRNAs closest to the start ATG of the GPD1 gene and used the colonies established with them. gRNA1: AAAGTCTGCATTGTCGGCTC, gRNA2: TGCATTGCTACCCACGATCT.

QUANTIFICATION AND STATISTICAL ANALYSIS

Ribosome profiling data analysis

Despite an rRNA depletion step in the library preparation protocol, a substantial number of sequencing reads derived from rRNA. Bowtie2 was used to align the reads against mouse rRNA sequences. Only the non-aligned reads were used for further analysis with TopHat v1.4.0 (Trapnell et al., 2009) using the reference genome mm10. To analyze the differentially expressed genes we used Cuffdiff v2.2.1 with classic fpkm as library normalization method and a FDR of 0.1 (Trapnell et al., 2012). The heatmap was generated with clustvis (Metsalu and Vilo, 2015), is median centered with log2 fold changes. Gene ontology analysis was performed using DAVID (Huang et al., 2009). 2 NSCs and 3 BTSCs from independent tumors were used for this experiment.

RNA-seq data analysis

Raw reads from *Gpd1* sgRNA-knockout RNA-seq experiments were aligned to mm10 (ensemble version 86) by STAR (2.4.1d) with default parameters (Dobin et al., 2013). The aligned reads were quantified by the feature Counts in Rsubread package (Liao et al., 2013; Team, 2018). We used the R package DESeq2 to identify the differentially expressed genes with the option "cooksCutoff = FALSE" (Love et al., 2014). A false discovery rate of 0.05 (Benjamini-Hochberg correction) was used to select differentially genes. Control cells are 1 BTSC line used for Risobome profiling culture as 3 samples, the same for samples from gRNA1 or gRNA2 GPD1 KO cells.

Gene ontology analysis was performed by DAVID (v6.8) with differentially expressed genes defined with a more stringent false discovery rate of 0.005. The gene symbols and fold changes (KO/ control, log2 value) were used as input for the GSEA Preranked tool in GSEA (v3.0)(Subramanian et al., 2005).

Immunohistochemistry

At least 5 tumors from 5 individual mice were analyzed for each staining. From each tumor pictures were taken from 3 slices from different tumor regions. For the Ki67/GFP and the Ki67/RFP co-staining, for each tumor pictures were taken from three vibratome slices from RFP, GFP and from not fully GFP tumors. In the last case pictures were taken from regions with and without GFP from the same slice. To capture all the cells on the thicker vibratome sections Z-projections were used (ImageJ, Z-project). The n numbers apply to the number of animals. Three ROIs were defined and counted for every brain tumor slice (ImageJ and Zeiss Zen software). A One-Way ANOVA test (SigmaPlot) was used to calculate the significance.

GPD1-KO survival analysis

Mice were monitored by blinded personnel and sacrificed once they showed severe symptoms, e.g., weight loss, apathy, and neurological symptoms. The genotypes were analyzed after animals being sacrificed. All the injected mice were used to generate the Kaplan-Meier survival curve with SigmaPlot. N refers to animal number.

Differentiation assay neurosphere assay

The differentiation experiments were repeated three times for every cell line and three regions of interest of every slide were captured. The DAPI stained nuclei and the antibody stained cells were counted (ImageJ) and analyzed with a One-Way ANOVA test (SigmaPlot).

For the sphere assay 2000 dissociated cells were seeded into one well of a 24 well plate and grown in NSC medium for a week and imagined at day 4 and 7. A picture of the whole well was taken with a Zeiss widefield microscope and the neuroshperes were counted with ImageJ. The assay was repeated at least three times (n represents the number of wells) for every cell line and the significance was analyzed with a One-Way ANOVA test (SigmaPlot).

Limited dilution assay

The significance of the limiting dilution assay was analyzed with the ELDA online tool. 48 wells were used per cell line.

Metabolomics/lipdiomics data analysis

The raw data of metabolomics in negative mode were base-2 logarithm transformed and subsequently normalized by the quantile method. PCA were performed on the normalized data. Student's t test were applied to the any pair of NSCs, BTSCs and BTSCs-GPD1-KO groups (4 samples were used from each cell line) were and multiple comparisons were adjusted by the Benjamini-Hochberg correction in R. The Pubchem Id of Metabolites with adjusted P value $\leq$ 0.05 were used as input for MetaboAnalyst and Ingenuity Pathway Analysis (IPA) (Chong et al., 2018; Kim et al., 2016; Krämer et al., 2014). We employed the "Pathway Analysis" in MetaboAnalyst with "Home sapiens (KEGG)" library, "Hypergeometric Test" for "Over Representation Analysis" and "Relative-betweeness Centrality" for "Pathway Topology Analysis." In addition, the log2 fold changes and adjusted P value were supplied to IPA for pathway annotations. We ran the "Metabolomics Analysis" inside of "core analysis" with "Expr Log Ratio" as measurement type. The raw data of lipidomics collected in both positive and negative mode were processed separately in the normalization and pairwise Student's t test procedures, similar to the procedures on the metabolomics data. In addition, we tried to annotate as many as possible lipids with Human Metabolome Databasse ID (HMDBID) via searching against LIPID MAPS Structure Database or PubChem database (Kim et al., 2016; Wishart et al., 2018). We merged the differential analysis results of positive mode and negative mode. Lipids were selected wit adjusted P value $\leq$ 0.05 and related HMDBID were used as input for both MetaboAnalyst and IPA. The same parameters are used in these two toolsets as for metabolomics data.

Weighted Gene Coexpression Network Analysis (WGCNA) of Single-cell RNA-seq data

The processed data of the publication of Tirosh et al. (2016) and Venteicher et al. (2017) were downloaded from Gene Expression Omnibus (GEO) and converted to TPM and log2(TPM +1), while latter were used in the downstream analysis. Gpd1 expressing cells were selected with log2(TPM+1) > 1. Further, genes were filtered with the following thresholds: (1) expressed in more than three cells; (2) mean value > = 0.5: (3) standard deviation > = 2. We used the R package WGCNA to build the signed co-expression networks. Briefly, a signed adjacencies matrix was built from spearman correlation network with a soft threshold of 12 and converted to a robust Topological Overlap Matrix. Next, gene trees were constructed with "average" method form the topological matrix. The gene modules were identified by dynamic tree cut approach with minimum module size of 30. Lastly, modules with similar expression profiles were merged together with the parameter "cutHeight = 0.25." Gene co-clustered with Gpd1 were used in Gene Ontology enrichment analysis via DAVID.

Murine tumor samples

Murine HCC tumor samples were derived from DEN-treated mice (Pusterla et al., 2013), intrahepatic cholangiocarcinomas were generated by hydrodynamic tail vein injection of a Sleeping-Beauty Transposon plasmid encoding oncogenic Kras (pT3 EF-KrasG12D) and a CRISPR/Cas9 plasmid encoding a sgRNA targeting p53 (Tschaharganeh et al., 2014) in C57/Bl6 mice.

DATA AND CODE AVAILABILITY

ImgageJ is a free software and can be downloaded from the following link https://imagej.nih.gov/ij/.

Invitrogen's RNAi designer (https://rnaidesigner.thermofisher.com/rnaiexpress/), the CRISPR Design tool provided in GeCKO (http://zlab.bio/guide-design-resources), NCBI-Blast (https://blast.ncbi.nlm.nih.gov/Blast.cgi), the Galaxy server (https://usegalaxy.org/) and ELDA (Extreme Limiting Dilution Analysis, http://bioinf.wehi.edu.au/software/elda/) (Hu and Smyth, 2009) are free to use online tools. The accession number for the sequence reported in this paper is GEO: GSE110869, GSE110866, GSE110867, and GSE110868.